Check for updates

View Article Online
View Journal

Dalton Transactions

Accepted Manuscript

This article can be cited before page numbers have been issued, to do this please use: A. Maro, K. A. Czerwiska, B. Machura, L. R. Raposo, C. Rodrigues, A. Fernandes, J. Malecki, A. Szapa-Kula, S. Kula and S. Krompiec, *Dalton Trans.*, 2018, DOI: 10.1039/C8DT00558C.

This is an Accepted Manuscript, which has been through the Royal Society of Chemistry peer review process and has been accepted for publication.

Accepted Manuscripts are published online shortly after acceptance, before technical editing, formatting and proof reading. Using this free service, authors can make their results available to the community, in citable form, before we publish the edited article. We will replace this Accepted Manuscript with the edited and formatted Advance Article as soon as it is available.

You can find more information about Accepted Manuscripts in the author guidelines.

Please note that technical editing may introduce minor changes to the text and/or graphics, which may alter content. The journal's standard Terms & Conditions and the ethical guidelines, outlined in our author and reviewer resource centre, still apply. In no event shall the Royal Society of Chemistry be held responsible for any errors or omissions in this Accepted Manuscript or any consequences arising from the use of any information it contains.

ROYAL SOCIETY OF CHEMISTRY

rsc.li/dalton

View Article Online
DOI: 10.1039/C8DT00558C

Journal Name

ARTICLE

Spectroscopy, electrochemistry and antiproliferative properties of Au(III), Pt(II) and Cu(II) complexes bearing modified 2,2′:6′,2′′-terpyridine ligands. Impact of metal center and substituent incorporated into terpy framework

Received 00th January 20xx,
Accepted 00th January 20xx

DOI: 10.1039/x0xx00000x

www.rsc.org/

Anna Maroń[a], Katarzyna Czerwińska[a], Barbara Machura[a,*], Luis Raposo[b], Catarina Roma-Rodrigues[b], Alexandra R. Fernandes[b,*], Jan G. Małecki[a], Agata Szlapa-Kula[c], Slawomir Kula[d], Stanisław Krompiec[c]

Structural, spectroscopic and electrochemical properties of six complexes $[AuCl(L^1)](PF_6)_2 \cdot CH_3CN$ (**1**), $[AuCl(L^2)](PF_6)_2$ (**2**), $[PtCl(L^1)](BPh_4) \cdot CH_3CN$ (**3**), $[PtCl(L^2)](SO_3CF_3)$ (**4**), $[CuCl_2(L^1)]$ (**5**) and $[CuCl_2(L^2)] \cdot CH_3CN$ (**6**) with modified 2,2′:6′,2′′-terpyridine ligands, 4′-(4-methoxyphenyl)-2,2′:6′,2′′-terpyridine ($\mathbf{L^1}$) and 4′-(4-methoxynaphthalen-1-yl)-2,2′:6′,2′′-terpyridine ($\mathbf{L^2}$), were thoroughly investigated and significant role of the substituent (4-methoxyphenyl or 4-methoxynaphthalen-1-yl) and metal center was demonstrated. The naphthyl-based substituent was found to increase the emission quantum yield of luminescent Au(III) and Pt(II) complexes. Furthermore, the antiproliferative potential of the reported complexes was examined towards human colorectal (HCT116) and ovarian (A2780) carcinoma cell lines as well as towards normal human fibroblasts. Au(III) complex **2** and Cu(II) complex **5** were found to have a higher antiproliferative effect in HCT116 colorectal and A2780 ovarian carcinoma cells when compared with the Pt(II) complex with the same ligand (**4**). The order of cytotoxicity in both cell lines is **2** > **6** > **1** > **3** > **4**. Complex **2** seems to be the more cytotoxic towards HCT116 and A2780 cancer cell lines with IC_{50} values 300x and 130x higher in normal human fibroblasts compared to the respective cancer cells. The viability loss induced by the complexes agrees with Hoechst 33258 staining and the typical morphological apoptotic characteristics like chromatin condensation and nuclear fragmentation and flow cytometry assay. The induction of apoptosis correlate with the induction of reactive oxygen species (ROS). Fluorescence microscopy analysis indicate that after a 3 h incubation, complexes **1–4** are localized inside HCT116 cells and the high levels of internalization correlate with their cytotoxicity.

Introduction

In recent years, metal complexes based on 2,2′:6′,2′′-terpyridine (*terpy*) and 4′-substituted terpy ligands have been extensively investigated due to numerous remarkable applications in various fields, including catalysis,[1–8] molecular electronics,[9–13] supramolecular chemistry[14–18] and chemotherapy.[19–38]

In the field of anticancer drug design, a great deal of attention has been devoted to the Pt(II)- and Cu(II)-terpyridine complexes. Penta-coordinated polypyridyl copper(II) coordination complexes have been reported to efficiently cleave DNA,[28, 39–46] while square planar Pt–terpyridine complexes have been found to be very good G-quadruplex binders.[47–54] The studies revealed also crucial role of structural modification of 2,2′:6′,2′′-terpyridine for the cytotoxicity of metal-drugs against cancer-cell lines. The possibility of tuning the antitumor behaviour of the gold(III)-terpyridine complexes by attaching suitable substituent to the central pyridine ring of 2,2′:6′,2′′-terpyridine has been demonstrated for the square-planar $[AuCl(4'\text{-R-terpy})](PF_6)_2$.[36] In this case, the use of multidentate ligand (4′-R-terpy) allowed also to overcome the problem of relatively poor stability profile of gold(III) complexes under physiological conditions, which hampers the development of gold(III) complexes as cytotoxic and antitumor agents.[27, 55]

Herein, we present the synthesis, characterization and antiproliferative activity of six complexes incorporating 2,2′:6′,2′′-terpyridine ligand framework (Scheme 1).

[a] Department of Crystallography, Institute of Chemistry, University of Silesia, 9th Szkolna St., 40-006 Katowice, Poland. Email: barbara.machura@us.edu.pl
[b] UCIBIO, Departamento de Ciências da Vida, Faculdade de Ciências e Tecnologia, Universidade NOVA de Lisboa, Campus de Caparica, 2829-516 Caparica, Portugal. Email: ma.fernandes@fct.unl.pt
[c] Department of Inorganic, Organometallic Chemistry and Catalysis, Institute of Chemistry, University of Silesia, 9th Szkolna St., 40-006 Katowice, Poland.
[d] Department of Polymer Chemistry, Institute of Chemistry, University of Silesia, 9th Szkolna St., 40-006 Katowice, Poland

Electronic Supplementary Information (ESI) available: Intra- and intermolecular hydrogen bonds, π···π interactions, X—Y···Cg(J)(π-ring) interactions, IR spectra, ^{1}H NMR, ^{13}C NMR, COSY, HMBC and HMQC NMR, powder XPRD, UV-Vis spectra, excitation and emission spectra, supramolecular packing, cyclic voltammograms and DFT calculations of compounds. See DOI: 10.1039/x0xx00000x

Published on 04 April 2018. Downloaded by Fudan University on 04/04/2018 08:52:59.

Dalton Transactions Accepted Manuscript

View Article Online
DOI: 10.1039/C8DT00558C

Published on 04 April 2018. Downloaded by Fudan University on 04/04/2018 08:52:59.

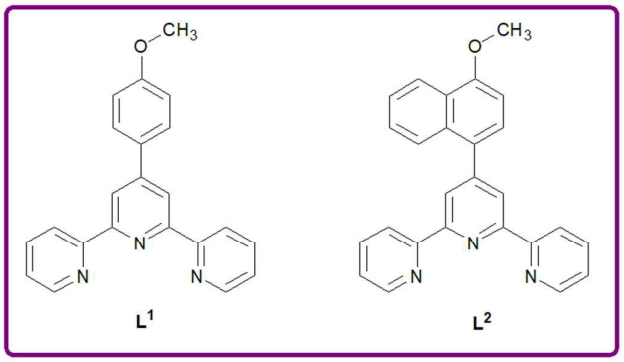

Scheme 1 Ligands used in the synthesis of the complexes. L^1 = 4′-(4-methoxyphenyl)-2,2′:6′,2′′-terpyridine, L^2 = 4′-(4-methoxynaphthalen-1-yl)-2,2′:6′,2′′-terpyridine

The main aim of this work was to investigate the effect of the coordinated 2,2′:6′,2′′-terpyridine ligand on the cytotoxicity of the complex as well as to compare the biological activity depending on metal centre. From structural point of view, comparison of $[PtCl(4'\text{-R-terpy})]^+$ and $[AuCl(4'\text{-R-terpy})]^{2+}$ seems to be especially interesting. The Au(III) coordination center is isoelectronic with Pt(II) and the complexes of both metals adopt a square-planar geometry.[56–58]

Results and discussion

Synthesis and general characterization of the complexes

The synthetic strategy of $[AuCl(L^1)](PF_6)_2 \cdot CH_3CN$ (**1**), $[AuCl(L^2)](PF_6)_2$ (**2**), $[PtCl(L^1)](BPh_4) \cdot CH_3CN$ (**3**), $[PtCl(L^2)](SO_3CF_3)$ (**4**) $[CuCl_2(L^1)]$ (**5**) and $[CuCl_2(L^2)] \cdot CH_3CN$ (**6**) is presented in Scheme 2. Reaction of $KAuCl_4$ with an equimolecular amount of 2,2′;6′,2′′-terpyridine derivative L^1 or L^2 (see Scheme 1) in methanol, followed by treatment with aqueous ammonium hexafluorophosphate afforded **1** and **2**, respectively. Syntheses of the platinum(II) complexes **3** and **4** were performed by Annibale's[59] and Dhara's[60] methods using $[PtCl_2((CH_3)_2SO)_2]$ and $[PtCl_2(PhCN)_2]$ as precursors, respectively. The copper(II) complexes (**5** and **6**) were isolated from the reaction of L^2 with $CuCl_2 \cdot 2H_2O$ in methanol.

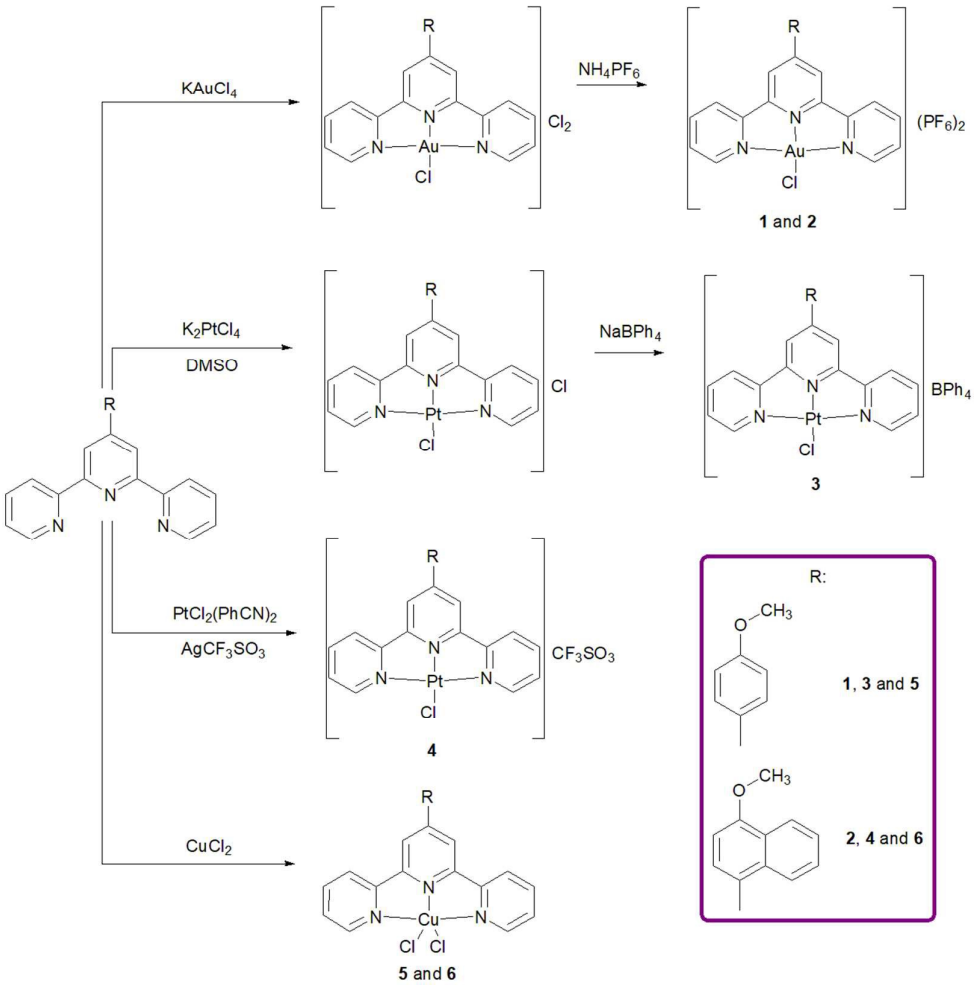

Scheme 2 Synthetic strategy of complexes **1**-**6**.

Dalton Transactions Accepted Manuscript

This journal is © The Royal Society of Chemistry 20xx

Please do not adjust margins
View Article Online
DOI: 10.1039/C8DT00558C

Published on 04 April 2018. Downloaded by Fudan University on 04/04/2018 08:52:59.

The IR spectra (see ESI Figure S1) of the ligands show characteristic bands in the range of 1600–1540 cm^{-1} assigned to ν(C=N) and ν(C=C) stretching vibrations. For all the metal complexes, these vibrations are only slightly shifted in comparison with those reported for the free ligand. Intense bands near 840 cm^{-1} and 558 cm^{-1} in the IR spectra of **1** and **2** are indicative of the presence of PF_6^- group.[61] Absorptions assignable to SO_3 part of SO_3CF_3 anion in **4** occur at 1268 cm^{-1} ($\nu_a(SO_3)$), 1029 cm^{-1} ($\nu_s(SO_3)$) and 638 cm^{-1} ($\delta_a(SO_3)$).[62] The coordination of the terpyridine ligand in **1**-**4** is also evidenced by ^{1}H NMR, ^{13}C NMR using COSY, HMBC and HMQC techniques (see Experimental and ESI Figures S2-S5). Expectedly, due to the impact of the metal-ligand bond, the signals assigned to the protons A1, A2 and A3 showed downfield shifts relative to the free ligand (see ESI Figures S6-S7 and Table S8). Also, distinctive singlets attributed to the methyl protons of the –OCH_3 group of **2** (4.15 ppm) and **4** (4.10 ppm) are shifted downfield with respect to **1** (3.97 ppm) and **3** (3.92 ppm). It is consistent with more extended π delocalization in the ligand $\mathbf{L^2}$.

Molecular structures

Perspective views of the asymmetric units of **1**–**4** and **6** are shown in Figure 1 (a-e), and the selected bond distances and

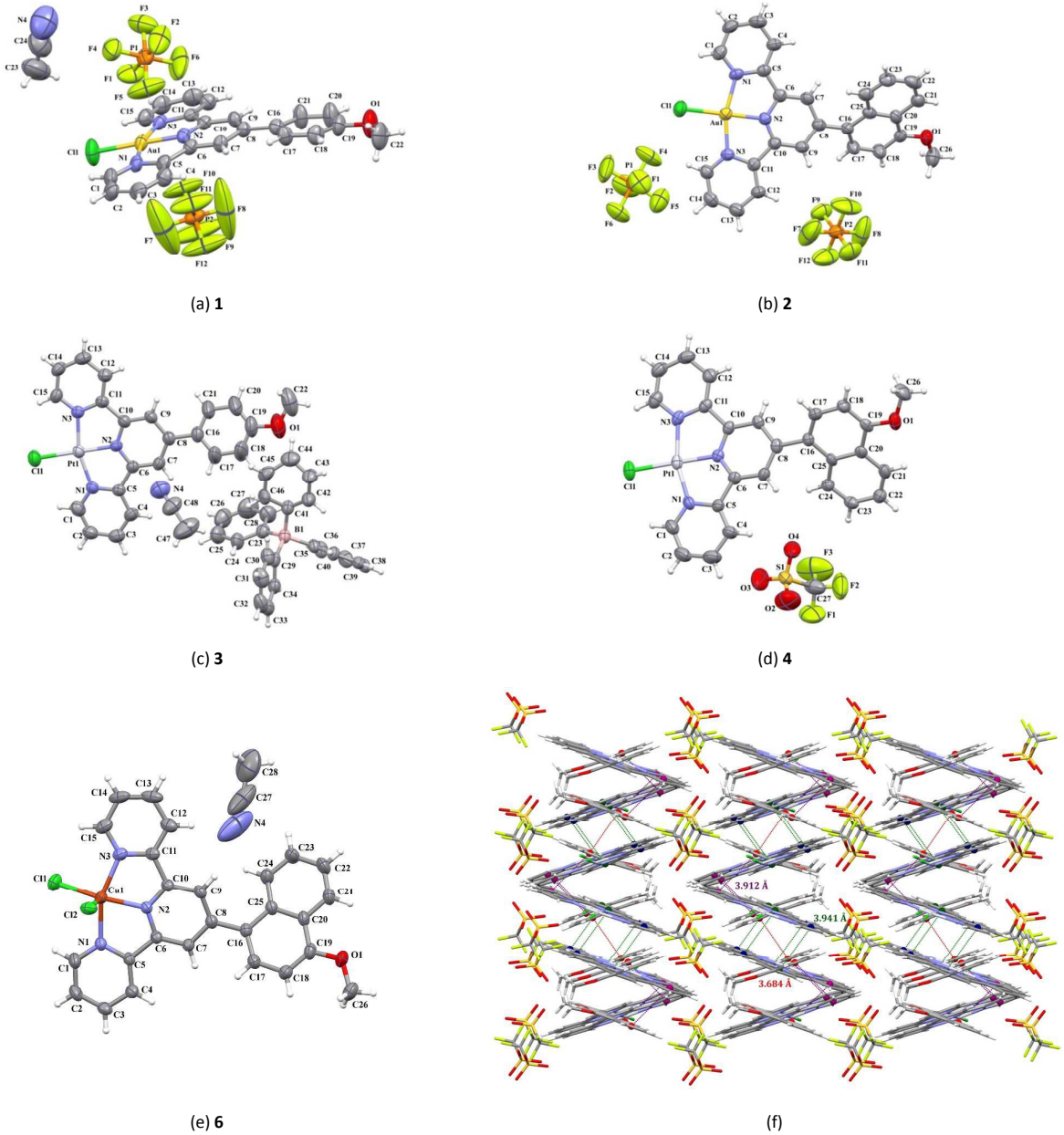

(a) **1** (b) **2** (c) **3** (d) **4** (e) **6** (f)

Figure 1 Molecular structures of **1**-**4** and **6** (a-e) together with the atom numbering. Displacement ellipsoids are drawn at 50% probability level. (f) Herringbone arrangement of the cations $[PtCl(L^2)]^+$ in **4.**

Dalton Transactions Accepted Manuscript

Please do not adjust margins

View Article Online
DOI: 10.1039/C8DT00558C

bond angles were included in Table 1. Noteworthy, despite many attempts, we were unable to successfully isolate the copper(II) complex with **L**^{1} in crystalline form.

The metal atom in the cations $[AuCl(L^n)]^{2+}$ and $[PtCl(L^n)]^{+}$ (n = 1 or 2) displays a distorted square planar coordination defined by three nitrogen atoms of the 4'-substituted 2,2';6',2''-terpyridine ligand (**L**^{1} or **L**^{2}) and chloride ligand. To evaluate the distortion from square planar, two parameters τ_4 and τ'_4 were calculated:[63, 64]

$$\tau'_4 = \frac{\beta - \alpha}{360° - \theta} + \frac{180° - \beta}{180° - \theta}$$

where α and β are two greatest valence angles, α < β, and $\theta = \cos^{-1}(-1/3) \approx 109.5°$. For ideal square planar and tetrahedral structures, the τ_4 and τ'_4 are 0 and 1, respectively. The distortion from square planar geometry increases in the order $[AuCl(L^1)]^{2+}$ (τ_4 = 0.1335 and τ'_4 = 0.0820) < $[PtCl(L^1)]^{+}$ (τ_4 = 0.1378 and τ'_4 = 0.0838) < $[AuCl(L^2)]^{2+}$ (τ_4 = 0.1378 and τ'_4 = 0.0883) < $[PtCl(L^2)]^{+}$ (τ_4 = 0.1481 and τ'_4 = 0.1038).

In **6**, the Cu(II) centre is penta-coordinated by the three N donor atoms of **L**^{2} ligand and two chloride ions. The angular

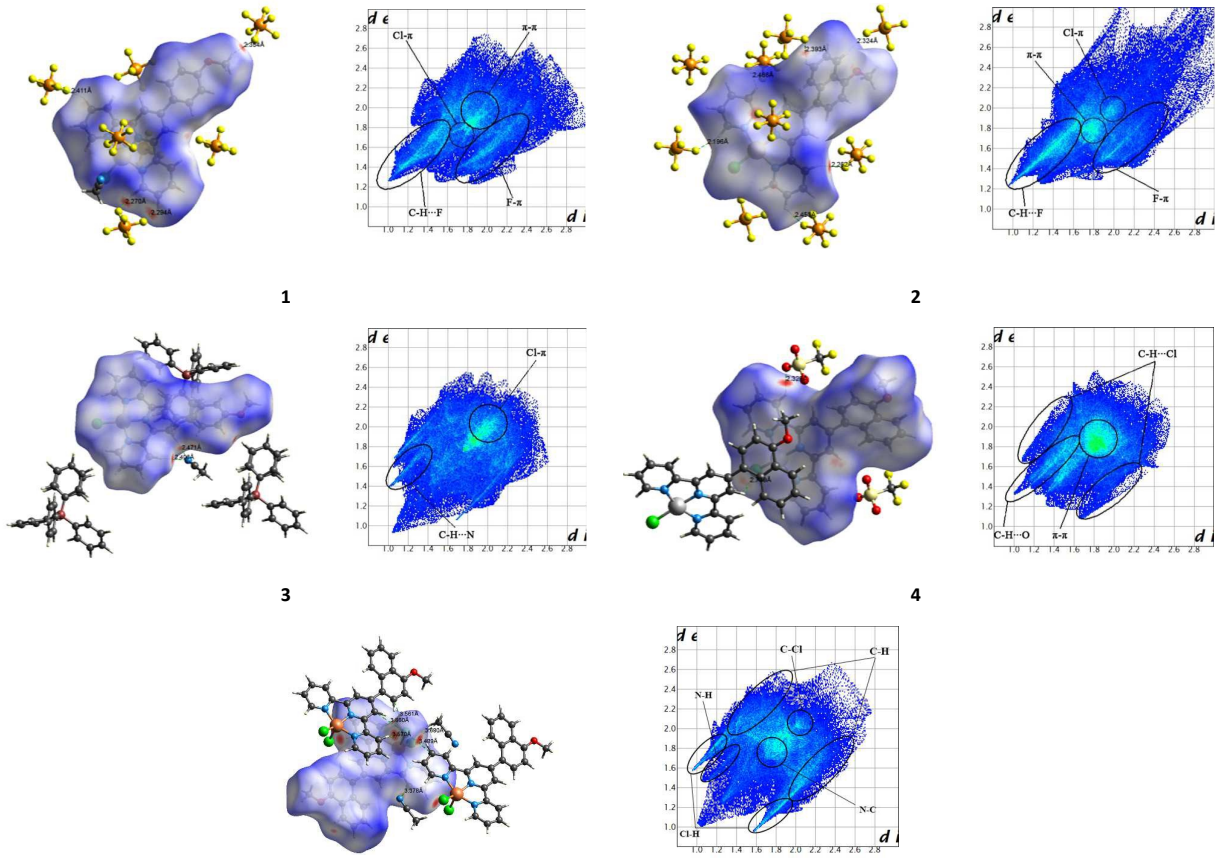

Figure 2 Hirshfeld surface mapped with d_{norm} (a) and 2D fingerprint plots (b) for **1**-**4** and **6**.

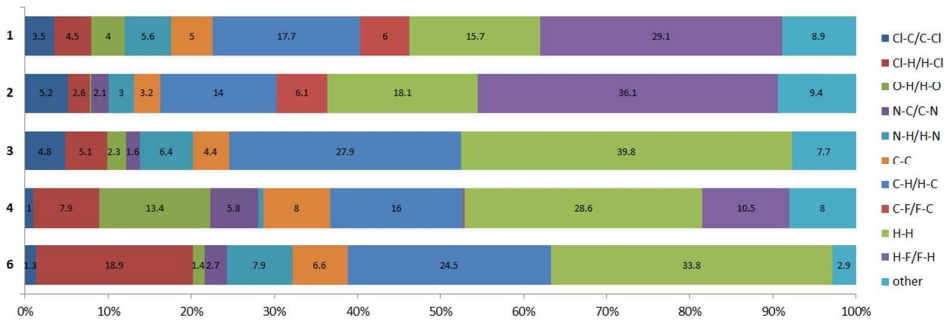

Figure 3 Relative contributions of various intermolecular interactions to the Hirshfeld surfaces for **1**-**4** and **6**.

This journal is © The Royal Society of Chemistry 20xx

Please do not adjust margins
Published on 04 April 2018. Downloaded by Fudan University on 04/04/2018 08:52:59.
Dalton Transactions Accepted Manuscript

Please do not adjust margins
View Article Online
DOI: 10.1039/C8DT00558C

Published on 04 April 2018. Downloaded by Fudan University on 04/04/2018 08:52:59.

Table 1 The selected bond lengths [Å] and angles [°] for **1**-**4** and **6**.

	1 (M=Au)	**2** (M=Au)	**3** (M=Pt)	**4** (M=Pt)	**6** (M=Cu)
Bond lengths [Å]					
M(1)–N(1)	2.024(6)	2.007(5)	2.015(4)	2.006(6)	2.044(2)
M(1)–N(2)	1.945(5)	1.954(5)	1.943(4)	1.927(5)	1.956(2)
M(1)–N(3)	2.021(6)	2.030(5)	2.017(4)	2.004(6)	2.040(2)
M(1)–Cl(1)	2.249(2)	2.2490(16)	2.3010(14)	2.2906(18)	2.2405(8)
M(1)–Cl(2)	–	–	–	–	2.4704(9)
Bond angles [°]					
N(1)–M(1)–N(2)	81.5(2)	81.5(2)	80.70(15)	80.7(2)	78.55(9)
N(1)–M(1)–N(3)	162.3(2)	162.3(2)	161.54(17)	162.4(2)	155.72(9)
N(2)–M(1)–N(3)	81.0(2)	80.9(2)	80.94(15)	81.7(2)	79.05(9)
N(1)–M(1)–Cl(1)	97.94(18)	98.65(16)	98.63(12)	99.02(17)	98.01(7)
N(2)–M(1)–Cl(1)	178.89(18)	178.27(16)	179.01(11	176.71(17)	155.21(8)
N(3)–M(1)–Cl(1)	99.55(17)	99.01(15)	99.70(12)	98.58(17)	98.38(7)
N(1)–M(1)–Cl(2)	–	–	–	–	98.14(8)
N(2)–M(1)–Cl(2)	–	–	–	–	98.96(7)
N(3)–M(1)–Cl(2)	–	–	–	–	94.47(7)

structural index parameter τ_5[65], expressed as the difference between the two largest angles divided by 60°, has a value of 0.085. Compared with the ideal values of 1 for a trigonal bipyramid and 0 for a square pyramid, the τ = 0.085 indicates that the geometry of the metal centre in **6** may be described as a slightly distorted square-pyramid.

The angular distortion from the idealized square planar geometry in cations $[AuCl(L^2)]^{2+}$ and $[PtCl(L^2)]^{+}$ and square-pyramid in the neutral $[CuCl_2(L^2)]$ may be attributed to geometrical constraints issued from the occurrence of two fused five-member chelate rings of the tridentate 4'-substituted terpyridyl ligand, resulting in N(1)–M(1)–N(2) and N(2)–M(1)–N(3) (M = Au, Pt) angles of 81.5(2)° and 81.0(2)° for **1** and 81.5(2)° and 80.9(2)° for **2**, 80.70(15)° and 80.94(15)° for **3**, 80.7(2)° and 81.7(2)° for **4** and 78.55(9)° and 79.05(9)° for **6**, respectively (Table 1).

In the complexes **1**–**4** and **6**, the terpy framework shows good planarity, the dihedral angles between the inner and outer pyridyl rings are 3.5(4)° and 5.4(4)° for **1**, 4.8(5)° and 7.0(4)° for **2**, 2.0(5)° and 2.0(9)° for **3**, 2.5(2)° and 3.3(4)° for **4** and 7.0(2)° and 8.3(7)° for **6**. The most striking difference between L^1 and L^2 ligand concerns the twist angle for the substituent ring with respect to the central ring of the terpy framework. While the 4-methoxyphenyl in **1** and **3** retains near coplanar with the central pyridine plane, 7.0(8)° in **1** and 8.3(8)° in **3**, the angle between the naphthyl plane and that of the central pyridyl ring is 46.2(7)° in **2**, 39.7(9)° in **4** and 30.0(2)° in **6**.

In all the examined complexes, the M–N bond of the central pyridyl ring of ligand is shorter than those of the outer pyridyl rings, which may be attributed to the constrained bite of the terpyridyl-based ligand. Typically for the square-pyramidal configuration, due to Jahn Teller distortion[66], the Cu–Cl apical bond in **5** is longer than the Cu–Cl basal bond. To some extent, however, an elongation of the Cu(1)–Cl(2) bond in **6** may be also caused by the participation of the Cl(2) atom in the formation of weak C—H···Cl interactions C(4)—H(4)···Cl(2), C(7)—H(7)···Cl(2), C(13)—H(13)···Cl(2) and C(17)—H(17)···Cl(2) (D···A distances = 3.570(3)Å, 3.661(3)Å, 3.489(3)Å and 3.561(3)Å respectively, with D—H···A angles = 165.00°, 150.60°, 151.60° and 154.60°, see Figure S17, ESI)

A summary of the intermolecular contacts in **1**–**4** and **6** crystal structures is provided in ESI, Tables S1-S3 as well as in spots of Hirshfeld surfaces[67–69] mapped with d_{norm} and in two-dimensional (2D) fingerprint plots (Figure 2). The relative contributions of various intermolecular interactions to the Hirshfeld surfaces are illustrated in Figure 3. As shown in Figures 2 and 3, weak hydrogen bonds C–H···F, C–H···N or C–H···O together with π-stacking interactions occur in the examined crystal structures. The strongest $\pi\cdots\pi$ contacts were revealed for **4** (Cg(N(1)/C(1)/C(2)/C(3)/C(4)/C(5))··· Cg(C(20)/C(21)/C(22)/C(23)/C(24)/C(25)) [symmetry code: *x*, 1/2-*y*, 1/2+*z*]; Cg(N(2)/C(6)/C(7)/C(8)/C(9)/C(10)) ··· Cg(N(3)/C(11)/C(12)/C(13)/C(14)/C(15)) [symmetry code: -*x*, -*y*, -*z*] and Cg(C(20)/C(21)/C(22)/C(23)/C(24)/C(25)) ··· Cg(C(20)/C(21)/C(2)/C(23)/C(24)/C(25)) [symmetry code: -*x*, -*y*, -1-*z*]). The cations $[PtCl(L^2)]^{+}$ in **4** adopts herringbone arrangement and form antiparallel chains as shown in Figure 1 (f). The distances Pt···Pt of 4.773 Å and 8.266 Å give evidence of no significant metallophilic interactions in the crystal. In the structure **3**, the cations $[PtCl(L^1)]^{+}$ form dimers through Cl···π interactions (Pt(1)-Cl(1)···Cg(N(1)/C(1)/C(2)/C(3)/C(4)/C(5)) [symmetry code: 1-*x*, 1-*y*,-*z*] and Pt(1)-Cl(1)···Cg(N(3)/C(11)/C(12)/C(13)/C(14)/C(15)) [symmetry code: 2-*x*,1-*y*,-*z*]) and stack in a head-to-tail fashion forming chain motifs with altering Pt···Pt distances of 3.499 Å and 4.549 Å (Figure S16, ESI). This crystal packing motif has been commonly seen in related Pt-terpy complexes[70]. The smaller Pt···Pt distance is indicative of weak metal-metal interaction. The value of *ca.* 3.5 Å is usually taken as the upper limit for a significant $d_z^2\cdots d_z^2$ interaction between two platinum atoms. [71–72] The shortest Au···Au distances (8.341 Å in **1** and 8.075 Å in **2**) are too long to indicate any significant attraction between individual metal centre (Figures S14 and S15, ESI).

Electronic absorption spectra and stability of gold(III) complexes

Absorption spectra of **1**–**6** in CH_3CN ($c = 5\cdot10^{-5}$ M) are shown in ESI, Figure S9, and the spectroscopic data are summarized in Table 2. For all the complexes, the vibronically structured high-energy absorption bands (between 250 and 350 nm) are attributed to $\pi\rightarrow\pi^*$ and $n\rightarrow\pi^*$ intraligand (IL) transitions associated with the coordinated terpyridyl ligand (see Figure

Table 2 The absorption maxima and molar extinction coefficient values for the free ligands (L^1 and L^2) and complexes **1**–**6** in acetonitrile.

Complex	λ/nm (10^4 ε/ $dm^3\cdot mol^{-1}\cdot cm^{-1}$)
1	264 (1.86), 275 (1.84), 287 (1.84), 296 (2.52), 353 (1.06), 382(1.33), 419 (1.72)
2	263 (1.25), 298 (2.07), 347 (0.99), 367 (0.78), 493 (0.76)
3	270 (0.85), 312 (0.57), 378 (0.38)
4	253 (2.4), 283 (2.67), 302 (1.71), 315 (1.62), 338 (1.33), 423 (0.85)
5	257 (1.29), 288 (1.19), 339 (1.33), 708 (0.13)
6	257 (2.11), 289 (1.60), 324 (1.66), 369 (0.85), 761 (0.13)
L^1	195 (4.44), 226 (2.34), 255 (2.11), 284 (3.70)
L^2 [72]	209 (1.72), 236 (1.58), 289 (0.87), 326 (0.55)

Dalton Transactions Accepted Manuscript

Please do not adjust margins

View Article Online
DOI: 10.1039/C8DT00558C

Published on 04 April 2018. Downloaded by Fudan University on 04/04/2018 08:52:59.

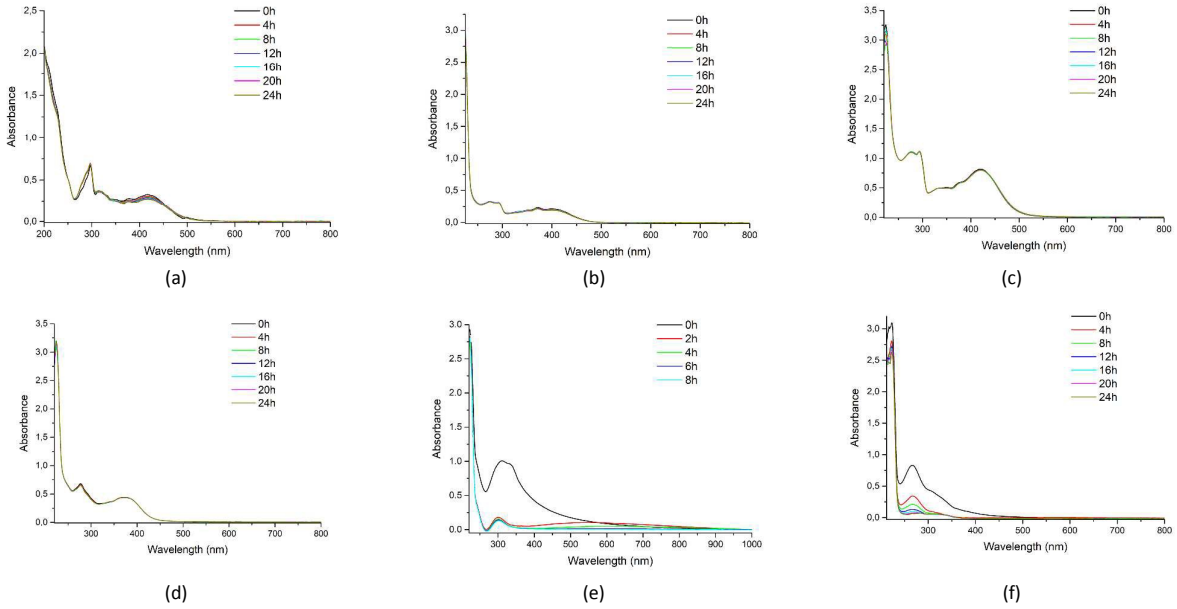

Figure 4 UV-Vis absorption spectra of **1** in CH_3CN (a), PBS buffer (pH 7.4, 130 mM NaCl) (b), CH_3OH:CH_3CH_2OH (1:4 v/v) (c), PBS upon addition of stoichiometric amount of glutathione (d), PBS upon addition of excess of glutathione (e) and PBS in the presence of sodium ascorbate (f). Spectra were recorded once every two or four hours for 8 or 24 h.

S10 in ESI).[73] With reference to the previous studies of Au(III)[74–80] and Pt(II)[81–87] complexes, the absorptions at lower energy (350–600 nm) are tentatively assigned to ligand-to-metal charge-transfer (LMCT) in **1** and **2** and metal-to-ligand charge-transfer (MLCT) in **3** and **4**. The broad and weak band in the visible region (with maximum at 761 nm) in the spectrum of **5** is attributed to overlapping $d_{xy}\rightarrow d_{x^2-y^2}$, $d_{yz},d_{xz}\rightarrow d_{x^2-y^2}$ and $d_{z^2}\rightarrow d_{x^2-y^2}$ transitions between d orbitals of the coordinated copper(II) ion.[88–90] The electron donating properties of the 4-methoxy-1-phenyl and 4-methoxy-1-naphthyl substituents may facilitate also intraligand charge transfer transitions (ILCT).

It is noteworthy that the CT absorptions of Au(III) and Pt(II) complexes are remarkably sensitive to the substituent at 4′-position of terpy ligand. With regard to $[AuCl(terpy)](PF_6)_2$[36] (373 nm) and $[PtCl(terpy)](SO_3CF_3)$[86] (391 nm), the lowest energy absorption band of the examined complexes is red-shifted. What is more, introduction of the larger aryl substituent (**2** and **4**) induces a further substantial shift to longer wavelength. As shown in Table 2 and ESI Figure S9, the low-energy band of **2** and **4** appeared at 74 and 45 nm longer in wavelength than that for **1** and **2**, respectively. The origin of the absorption bands of **1–4** was also considered with the aid of DFT and TD-DFT calculations. The energies and characters of the selected singlet electronic transitions, together with assignment to the experimental absorption bands are presented in Figure 5 as well as Tables S4–S7 and Figure S20 in ESI. For the complexes **1** and **2**, dominant contribution to the longest wavelength band is attributed to one-electron excitation HOMO→LUMO+1 with large value of oscillator strength, shifted in the direction of lower energies in relation to the maximum of the experimental band. It is a substituent-to-terpyridine charge transfer transition, ^{1}ILCT. The HOMO is

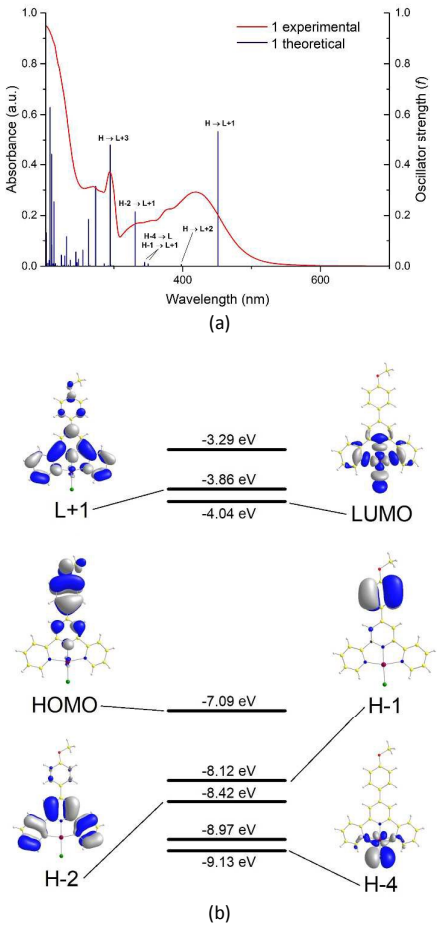

Figure 5. (a) Experimental absorption spectrum (red line) with calculated transitions (navy blue); (b) Graphical representations of selected MOs and their TD-DFT energies for **1**.

This journal is © The Royal Society of Chemistry 20xx

Dalton Transactions Accepted Manuscript

Please do not adjust margins
View Article Online
DOI: 10.1039/C8DT00558C

Published on 04 April 2018. Downloaded by Fudan University on 04/04/2018 08:52:59.

predominately constituted by π orbitals of 4-methoxy-1-phenyl or 4-methoxy-1-naphthyl substituent, while LUMO+1 was found to be distributed primarily over 2,2′:6′,2′′-terpyridine skeleton. As demonstrated by DFT calculations, 4-methoxy-1-naphthyl substituent destabilizes the HOMO orbital, stabilizes the LUMO, while the LUMO+1 energy remains almost unchanged (Figure S20 (a-b), ESI), which is manifested as a red-shift in absorption spectra upon replacement of 4-methoxy-1-phenyl (in **1**) for 4-methoxy-1-naphthyl (in **2**). For both Au(III) complexes, the LUMO presents significant $5d_{x^2-y^2}$ gold character and contribution of HOMO→LUMO transition is negligible in the lowest energy band. Absorptions in the range 300–400 nm are attributed to the overlapping transitions of LMCT, ILCT, ^{1}LLCT and $\pi_{terpy}\rightarrow\pi^*_{terpy}$ (LE, locally excited) in nature.

For the complexes **3** and **4**, the low energy absorption band is dominated by the excitation HOMO→LUMO assigned to ^{1}MLCT and ^{1}ILCT (Figure S20 (c-d) and Table S6-S7, ESI). The LUMO of **3** and **4** is delocalized over 2,2′:6′,2′′-terpyridine skeleton, with participation of π^*_{terpy} of 79% for 3 and 80% for 4, while the HOMO is contributed by π orbitals of the substituent R (57% for **3** and 75% for **4**) along with contributions from $5d_\pi$ platinum (17% for **3** and 5% for **4**) and π_{Cl} (5% for **3** and 1% for **4**) components.

In analogy to the Au(III) complexes, naphthyl substituent destabilizes the HOMO orbital, which is manifested in the bathochromic shift of the lowest energy absorption of **4** in relation to **3**. Furthermore, replacement of 4-methoxy-1-phenyl by 4-methoxy-1-naphthyl leads to decrease in contribution of Pt(II) *d* orbitals in the HOMO, resulting in predominant ILCT character of the lowest energy absorption for **4**. Higher energy absorption bands of **3** and **4** are attributable to ^{1}MLCT, ^{1}ILCT and $^1(\pi_{terpy}\rightarrow\pi^*_{terpy})$ excited states.

Taken into consideration that Au(III) complexes are sensitive to hydrolysis, solutions of **1** and **2** in in acetonitrile and phosphate buffered saline (PBS buffer) were examined spectrophotometrically over 24 hours. As shown in Figures 4 and S11 (ESI), the intensity of the absorptions bands was almost at the same level during 24 h indicating stability of Au(III) complexes in CH_3CN and PBS solutions, and in this last case, indicating that further biological studies can be pursuit. Slight spectral changes were observed for 24 h in PBS buffer following addition of stoichiometric amount of the biologically important reducing agent glutathione. In contrast, sodium ascorbate and excess of glutathione were found to cause rapid reduction of both **1** and **2**, accompanied by disappearance of the LMCT band (Figures 4(e-f) and S11(e-f) ESI). As there was no increase in absorbance between 500 and 600 nm, typical for colloidal gold(0), conversion from gold(III) to gold(I) can be postulated for **1** and **2** in PBS upon exposure of sodium ascorbate.[91–92]

Photoluminescence

The photoluminescence properties of the complexes **1–5** and corresponding ligands[73] were investigated in acetonitrile solutions at ambient conditions as well as in rigid matrices at 77 K (Table 3 and Figure 6). The emission of the free ligands is strongly affected by changes in solvent polarity (Figure S13, ESI). No vibronic structure and significant red-shift of the fluorescence on passing from non-polar to polar solvent may indicate a charge-transfer character of the excited state in the case of $\mathbf{L^1}$ and $\mathbf{L^2}$. Considering the molecular structure of $\mathbf{L^1}$ and $\mathbf{L^2}$, the ILCT process occurs when an electron is transferred from the electron-rich 4-methoxy-1-phenyl or 4-methoxy-1-naphthyl substituent to the *terpy* moiety.

To examine the CT character of the excited state of the free ligands, the difference between the excited and ground state dipole moments ($\Delta\mu=\mu_e-\mu_g$) was estimated using the Lippert–Mataga equation (eqn (1)), where $\Delta E_{exc\text{-}em}$ is Stokes shift (cm^{-1}), *h* is the Planck's constant, *c* is the speed of light in vacuum, *a* is the Onsager cavity radius, and Δ*f* is the orientation polarizability of the solvent, which measures both electron mobility and dipole moment of the solvent molecule. Δ*f* was calculated using equation (2), where ε is the dielectric constant of the solvent, n – the optical refractive index of the solvent. Onsager cavity radii (*a*) were calculated theoretically with use of the Gaussian09[93].

Table 3 Photoluminescence properties of complexes.

Complex	Medium	λ_{PE} [nm]	λ_{PL} [nm]	Φ_{PL} [%]	τ_{eff} [ns] [τ_n [ns] (weight, %)]	χ^2
1	CH_3CN	315, 388	515	1.12	**4.18** [4.41 (94.84%), 0.05 (5.16%)]	1.157
	CH_3OH:C_2H_5OH	342	457, 485, 503	—	**520** [184.4 (96.58%), 10000 (3.42%)]	1.067
2	CH_3CN	334, 361 (sh), 391	626	5.64	**1.60** [1.33 (81.05%), 2.77 (18.95%)]	1.097
	CH_3OH:C_2H_5OH	324, 338, 371	I: 441	—	I: **4.79** [5.28 (90.67%), 0.02 (9.33%)]	1.251
			II: 513, 557		II: **1079** [340 (84.20%); 5010 (15,80%)]	1.115
3	CH_3CN	334, 394	567	4.27	**20.12** [28.11 (71.37%), 0.22 (28.63%)]	0.900
	CH_3OH:C_2H_5OH	343, 423	560, 600, 650 (sh)	—	**45718** [59980 (54.23%), 28820 (45.77%)]	1.112
4	CH_3CN	366, 465	688	5.94	**103.39** [119.39 (86.08%), 4.45 (13.92%)]	0.955
	CH_3OH:C_2H_5OH	302, 317, 340, 428	567, 607 (sh)	—	**90129** [63654 (60.86%), 131295 (39.14%)]	1.217
$\mathbf{L^1}$	CH_3CN	253, 281, 293	385	25.10	**2.15** [2.15 (100%)]	1.079
	CH_3OH:C_2H_5OH	254, 276, 294	I: 338, 355, 372	—	I: **3.56** [3.56 (100%)]	1.068
			II: 442, 472, 503		II: **21987** [79.90 (79.54%), 107154 (20.46%)]	1.194
$\mathbf{L^2}$ [72]	CH_3CN	259, 342	432	12.00	**4.14** [4.14 (100%)]	1.129
	CH_3OH:C_2H_5OH	323	I: 375	—	I: **1.82** [2.13 (84.51%), 0.10 (15.43)]	1.088
			II: 507, 542, 582		II: **6089** [192.88 (90.79%), 64212 (9.21)]	1.182

Dalton Transactions Accepted Manuscript

Please do not adjust margins

View Article Online
DOI: 10.1039/C8DT00558C

Published on 04 April 2018. Downloaded by Fudan University on 04/04/2018 08:52:59.

$$\Delta E_{exc-em} = \frac{2(\mu_e-\mu_g)^2}{hca^3}\Delta f + Const. \quad (1)$$

$$\Delta f = \frac{\varepsilon-1}{2\varepsilon+1} - \frac{n^2-1}{2n^2+1} \quad (2)$$

The calculated values of $\Delta\mu$ are 14.77 D and 16.56 D for **L^1** and **L^2**, respectively. The higher $\Delta\mu$ value obtained for **L^2** is indicative of greater ILCT character in the excited state.

Except for **5** and **6**, all the studied complexes were luminescent (see Figure S12, ESI). In acetonitrile solutions, structureless emission bands were observed at λ_{max} = 515, 626, 567 and 688 nm for **1–4**, respectively (Figure 6 (a)). The emission lifetimes fall in the nanosecond time regime and the luminescence quantum yields are in the range 1.12–5.94 %. Most interestingly, upon replacement 4′-(4-methoxyphenyl)-2,2′:6′,2′′-terpyridine (**L^1**) by 4′-(4-methoxy-naphthalen-1-yl)-2,2′:6′,2′′-terpyridine (**L^2**), the emission shifts to lower energies (from 515 nm for **1** to 626 nm for **2** and from 567 nm for **3** to 688 nm for **4**), attributable to the increased extent of π-delocalization in the larger aromatic system of **L^2**.[82, 94–95] It is consistent with the trends observed for the free ligands **L^1** and **L^2.**

For both Au(III) and Pt(II) complexes, the red shift is accompanied by an increase in luminescence quantum yield.[82–83, 96–98] In line with previous findings[75, 83, 86, 96, 99–100] the rather broad and structureless emission bands of **1–4** in acetonitrile may be indicative of the excited state with significant CT character. Such assignment is supported by the theoretical calculations revealing significant contribution of the ILCT excited states, especially for Au(III) complexes. Owing to low solubility of **1–4**, however, it was impossible to investigate solvent effects on the emission. The nanosecond range of lifetimes supports fluorescent nature of these emissions. It should be also noted that **1** and **2** are very rare examples of non-cyclometalated gold(III) complexes that are emissive in fluid solution at room temperature.[92]

In a rigid glass at 77 K, the emission bands of **1–4** display appearance of partial vibronic coupling features and they are generally shifted to higher energies compared to acetonitrile solutions. Considering the large Stokes and long emission lifetimes, the emissions of the Pt(II) complexes (**3** and **4**) could be attributed to phosphorescence. With reference to earlier reports and theoretical calculations, it can be assumed that the luminescence of **3** and **4** originates from ^{3}MLCT and ^{3}LC excited states.

The photophysical behaviour of the complex **2** is strikingly different from that of **1**. The compound **2** is a rare example of coordination complex with 5d metal centre, in which intersystem crossing (ISC) is not fast enough to eliminate the fluorescence. It displayed both fluorescence (441 nm, τ_{eff} = 4.79 ns) and phosphorescence (499 nm, 550 nm; τ_{eff} = 1079 ns), while the emission of **1**, with maxima at 457 nm, 485 nm, 503 nm and effective emission lifetime of 520 ns, is assigned to phosphorescence. The higher-energy band of **2** is suggested to be of singlet origin and ILCT character. Compared to the free ligand **L^2**, the band is red-shifted by 66 nm, which is attributed to the impact of metal center (Figure 6 (c)). The structured bands of **1** and **2**, at lower energy and associated with a longer

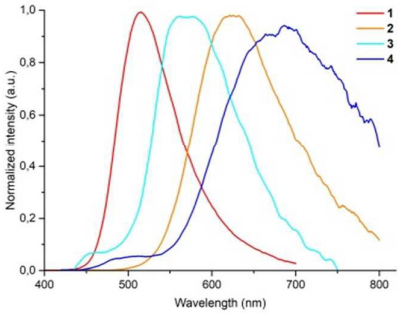

(a)

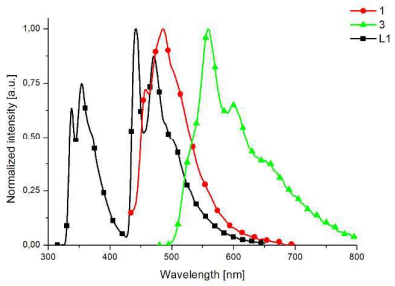

(b)

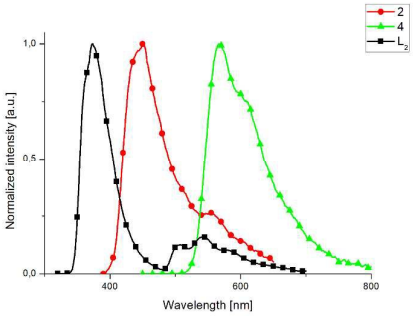

(c)

Figure 6 Emission spectra of complexes in CH_3CN (a) and in CH_3OH:CH_3CH_2OH (1:4 v/v) rigid matrices (b and c).

lifetime, are proposed to be of $^3(\pi\rightarrow\pi^*)$ character. They fall in the same energetic region as that for the free ligands (Figure 6 (b-c)). The possibility of emissive impurities in the samples was excluded on the basis of stability studies of **1** and **2** in CH_3OH:C_2H_5OH (1:4 v/v) (Figure 4), indicating no dissociation of the coordinated terpyridine ligand.

The fluorescent/phosphorescent emission in 4d/5d transition metal complexes are of great fundamental interest.[101–105] Due to strong spin-orbit coupling which facilitates intersystem crossing (ISC) from the singlet to the triplet state, these phenomena are rarely observed in organometallic and coordination complexes with heavy transition-metal centres.[99] Recently, Chi and Chou and co-workers performed a detailed study of dual emission in a series of osmium complexes,[103–104] showing the impact of π-conjugated aromatic system appended to β-diketonate ligand on the proportion of

Dalton Transactions Accepted Manuscript

This journal is © The Royal Society of Chemistry 20xx

Please do not adjust margins
View Article Online
DOI: 10.1039/C8DT00558C

Published on 04 April 2018. Downloaded by Fudan University on 04/04/2018 08:52:59.

Table 4 Electrochemical properties of complexes.

Complex	E_{red1} [V]	E_{red2} [V]	$E_{red1onset}$ [V]	$E_{red2onset}$ [V]	EA [eV][a]	E_{ox1} [V]	E_{ox2} [V]	E_{ox3} [V]	$E_{ox1onset}$ [V]	$E_{ox2onset}$ [V]	$E_{ox3onset}$ [V]	IP [eV][a]	E_g [eV]
1	-0.48	-1.10	-0.19	-1.00	-4.91	1.07	1.67	—	0.90	1.49	—	-6.00	1.09
2	-0.32	-1.11	-0.20	-1.00	-4.90	1.18 *(0.19)*[b]	—	—	1.07	—	—	-6.17	1.27
3	-1.32 *(0.23)*	-1.76 *(0.13)*[b]	-1.11	-1.72	-3.99	0.38 *(0.25)*	1.17	—	0.35	0.99	—	-5.45	1.46
4	-1.22 *(0.14)*[b]	-1.77 *(0.08)*[b]	-1.12	-1.71	-3.98	1.14 *(0.11)*[b]	—	—	1.08	—	—	-6.18	2.20
5	-0.57 *(0.07)*[b]	-1.18	-0.44	-0.96	-4.66	0.98	—	—	0.74	—	—	-5.84	1.18
6	-0.63 *(0.06)*	-1.30	-0.41	-1.02	-4.69	0.92	1.19	—	0.77	1.08	—	-5.87	1.18
L_1	-2.51 *(0.30)*[b]	—	-2.36	—	-2.74	1.27	1.43	1.57	1.17	1.34	1.49	-6.27	3.53
L_2	-2.46	—	-2.32	—	-2.78	1.16 *(0.09)*[b]	—	—	0.96	—	—	-6.06	3.28

[a] obtained using following equation EA = -5.1 – $E_{red1onset}$; IP = -5.1 - $E_{ox1onset}$; [b] (E_{pc}-E_{pa} [V])

fluorescence to phosphorescence. In turn, fluorescence has been well documented for transition-metal complexes containing fused aromatic systems such as perylene, perylene diimide, pyrene and tetracene.[106–110] Lack of the phosphorescence in these systems suggests that the rate of intersystem crossing to the triplet state is much slower than the radiative rate of fluorescence.

Electrochemistry

The redox behaviour of **1–6** was investigated using the cyclic voltammetry (CV) methods. The electrochemical data, together with the calculated electron affinity and ionization potential and band gap, are gathered in Table 4. Moreover, Figures S18 and S19 in ESI show cyclic voltammograms (reductive and oxidative scans) of the studied complexes. The energy of the frontier molecular orbitals was calculated using the ferrocene (Fc) ionization potential value of -5.1 eV as the standard. The Au(III) complexes (**1** and **2**) show two irreversible reduction processes in acetonitrile solution. With the references to the previous studies,[76, 111] they can be attributed to the gold(III)→gold(I) and gold(I)→gold(0) processes, expected in non-aqueous solutions. $\mathbf{L^1}$ and $\mathbf{L^2}$ ligands are electroactive at potentials close to −2.5 V, which fall far away from the processes observed herein (see Table 4 and reference [73]). Furthermore, Au(III)→Au(I)→Au(0) reduction was also confirmed by the presence of a gold deposit on the electrode surface after the electrolysis (see Figure S18 in ESI). As the complex **2** is reduced at more positive potential, it can be assumed that the ligand $\mathbf{L^1}$ stabilized the Au(III) oxidation state against reduction slightly better than $\mathbf{L^2}$. The oxidation processes in **1** and **2** can be assigned as the ligand-centred oxidation.[73] Noteworthy, the first oxidation potential for complex **2** is slightly anodic shifted compared to **1**, which is consistent with the extended π-delocalization of $\mathbf{L^2}$ (in **2**) compared to $\mathbf{L^1}$ (in **1**).

Typical of Pt(II) terpyridyl complexes[12, 82, 84, 94, 112–114] the cyclic voltammograms of **3** and **4** exhibit a pair of reversible ligand-based reduction waves, appearing at much positive potentials compared to the free ligands $\mathbf{L^1}$ and $\mathbf{L^2}$. Noteworthy, the redox potentials of **3** (-1.32 V, -1.76 V) and **4** (-1.22 V, -1.77 V) are similar, which may suggest that electron changes upon electroreduction occur at π-deficient terpyridine core.[94] What is more, these values are very close to those reported for the related Pt(II) terpyridine complexes, [Pt(terpy)Cl]SO_3CF_3,[112] [Pt(terpy)Cl]TFPB,[84] [Pt(4'-SCH_3-terpy)Cl]TFPB,[84] [Pt(4'-CH_3-terpy)Cl]TFPB,[84] [Pt(4'-Ph-terpy)(CN)]SbF_6,[113] [Pt(terpy)(C≡$CC_6H_4NO_2$)]PF_6,[115] [Pt(4'-Ph-terpy)Cl]TFPB,[82] [Pt(4'-Np1-terpy)Cl]PF_6,[82] [Pt(4'-Np2-terpy)Cl]PF_6,[82] [Pt(4'-Phe9-terpy)Cl]PF_6,[82] [Pt(4'-Pyre1-terpy)Cl]PF_6[82] (where TFPB – tetrakis[3,5-bis(trifluoromethyl)phenyl]borate, Np1 – 1-naphthyl, Np2 – 2-naphthyl, Phe9 – 9-phenanthrenyl, Pyre1 – 1-pyrenyl). On the contrary to Au(III) complexes **1** and **2**, these potentials are not influenced by R substituent attached to the terpy at 4-position. In line with the above mentioned reports, it can anticipated that the delocalization onto the π system of the substituent counteracts its electron-donating effect, which results in the same reduction potential for **3** and **4**. The anodic peak observed at 0.35 V in the cyclic voltammogram of **3** is ascribed to the counterion $[BPh_4]^-$ [116]. The oxidation potential at 1.17 V for **3** and 1.14 V for **4** are relatively close to the potentials observed for one electron oxidation of the $\mathbf{L^1}$ (1.27 V) and $\mathbf{L^2}$ (1.14 V) ligands, therefore they can be assigned to the metal-perturbed ligand-centred oxidation (see Table 4 and reference [117]). Compared to literature data on platinum complexes,[115, 118–119] however, metal-centred oxidation from Pt(II) to Pt(III) assignment can be also taken into consideration. For complexes **5–6**, reversible (-0.57 V for **5** and -0.63 V for **6**) and irreversible (-1.18V for **5** and -1.30 V for **6**) reduction waves are associated with Cu(II)→Cu(I) and Cu(I)→Cu(0) processes. With reference to literature[120] the ligand-based reduction processes are expected to appear at much more negative potentials in Cu(II) terpyridyl complexes.

Dalton Transactions Accepted Manuscript

Please do not adjust margins

View Article Online
DOI: 10.1039/C8DT00558C

Published on 04 April 2018. Downloaded by Fudan University on 04/04/2018 08:52:59.

Cytotoxic potential of terpyridine derivatives and metal complexes

The dose response curves obtained for the terpyridine derivatives L^1, L^2 and the metal complexes **1–6** in HCT116 and A2780 cancer cell lines and in normal fibroblasts (Figure 7 and Figure 8) enabled the determination of the IC_{50}, a measure of the *in vitro* cytotoxicity expressed as the concentration of complex that inhibits proliferation of cells by 50% as compared with controls (IC_{50}; μM) (Table 5). As observed in Figures 7 and 8 both free ligands L^1 and L^2 display a very high cytotoxic activity with a very low IC_{50} (particularly L^2 < 1 μM) in all the tested cell lines including normal human fibroblasts (Table 5). This very high cytotoxicity in normal cells reduce their applicability in cancer therapy. However, when bound to the metal centres these cytotoxic effects in normal cells is reversed except for complex **5** (Figure 8 and Table 5). Indeed, this very high cytotoxicity of complex **5** in normal cells (higher than in A2780 and HCT116 cancer cells - Table 5) was a reason for not pursuing additional biological tests with this complex. Remarkably,

Table 5 Relative IC_{50} (48h) of ligands L^1 and L^2 and metal complexes **1**-**5** for cancer cell lines HCT116 and A2780 and normal human fibroblasts.

Cell Lines	L^1	L^2	1	2	3	4	5	6
HCT116	0.49 ±0.07	0.18 ±0.04	0.45 ±0.08	0.27 ±0.06	1.62 ±0.05	2.94 ±0.03	1.02 ±0.04	0.40 ±0.06
A2780	1.12 ±0.06	0.97 ±0.03	1.78 ±0.05	0.64 ±0.18	9.69 ±0.04	16.12 ±0.07	2.54 ±0.05	0.95 ±0.05
Fibroblasts	9.03 ±0.08	0.95 ±0.08	30.33 ±0.11	85.24 ±0.10	60.11 ±0.06	>100	<0.3	32.78 ±0.06

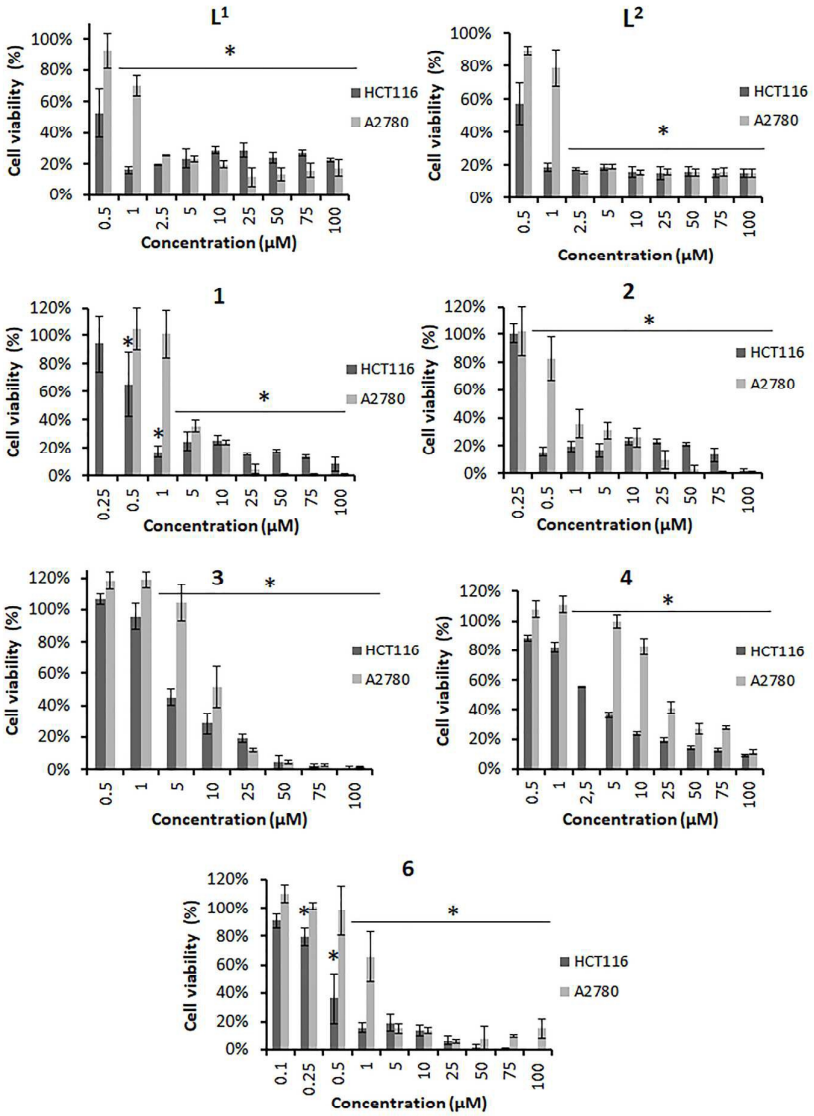

Figure 7 Cytotoxicity of ligands L^1 and L^2 and metallic complexes **1**-**5** in HCT116, and A2780 cell lines. Cells were incubated with increasing concentrations of complexes for 48 h and cell viability percentage was determined by the MTS assay, using cells incubated with 0.1% (v/v) DMSO as control. Results of complex **5** are not shown. The results shown are expressed as the mean ± SD from three independent assays. The symbol * means that the results are statistically significant with a $p < 0.05$ (as compared to control for each cell line).

Dalton Transactions Accepted Manuscript

This journal is © The Royal Society of Chemistry 20xx

Please do not adjust margins
View Article Online
DOI: 10.1039/C8DT00558C

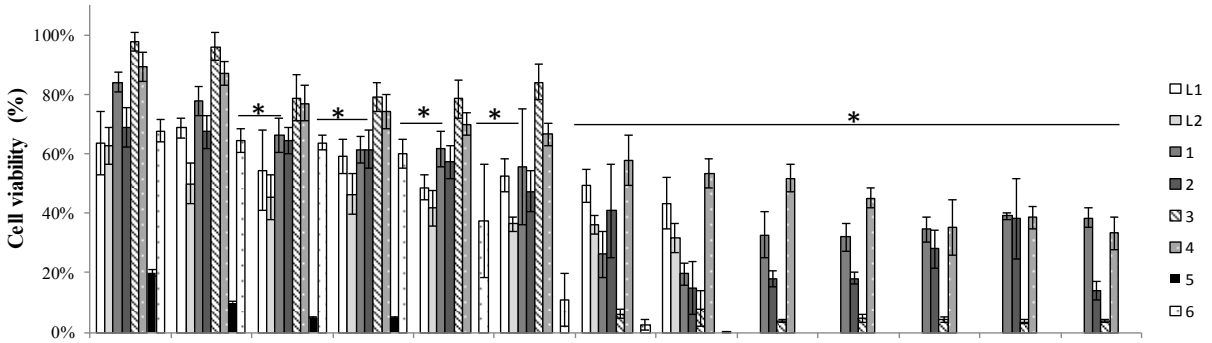

Figure 8 Cytotoxicity of ligands L^1 and L^2 and metallic complexes **1**-**6** in normal fibroblasts. As in Figure 7, cells were incubated with increasing concentrations of complexes for 48 h and cell viability percentage was determined by the MTS assay, using cells incubated with 0.1% (v/v) DMSO as control. The results shown are expressed as the mean ± SD from three independent assays. The symbol * means that the results are statistically significant with a $p < 0.05$ (as compared to control).

complexes **1-4**, **6** displayed a marked decrease in cytotoxicity when compared to the respective ligand has shown by the raise of the IC_{50} of normal fibroblasts (Table 5).

The Au(III) complex **2** presents a IC_{50} 300x and 130x higher in normal fibroblasts compared to HCT116 and A2780 cells respectively. Complex **2** presents the lowest IC_{50} for both cancer cell lines. Indeed, the IC_{50} cytotoxicity order is **2** > **6** > **1** > **3** > **4**. Comparing both Au(III) complexes their cytotoxicity follows their respective ligand cytotoxicity (L^2>L^1). The neutral Cu(II) complex **6** with L^2 is more cytotoxic compared to both Pt(II) complexes. Interestingly, Cu(II) and Au(III) complexes are more cytotoxic compared to Pt(II) complexes (Table 5). This higher cytotoxicity agrees with the above results concerning their redox potential and lower stability in PBS (for Au(III) complexes) or biological reducing environments[121]. This different cytotoxicity may also be due to different internalization rates and/or different mechanisms of action within cellular compartments. It is well known the effect of Cu(II) as a DNA cleaving agent.[30, 34] It is interestingly to note that in the same experimental conditions all the complexes display a higher cytotoxic activity in HCT116 cells compared to cisplatin, the common antitumor drug in clinical practice (IC_{50} = 15.20 ± 0.55 μM).[122] Additionally, to further validate these results, cell viability was also accessed by the trypan blue exclusion method in HCT116 and A2780 cells which also confirmed the metal complexes cytotoxicity (Figure S21).

The reduction of cell viability promoted by the complexes **1–4, 6** in HCT116 cells (Figure 7) prompted us to evaluate the underlined mechanisms of cell death. Apoptosis analysis was initially performed by staining with Hoechst 33258 dye due to its high affinity for DNA allowing the detection of nuclear alterations like chromatin condensation and nuclear fragmentation, typical features of apoptotic cells.[8] Hoechst 33258 staining of HCT116 cells after 48 h of exposure to the IC_{50} of each complex allowed us to observe a reduction in the number of stained cells compared to control cells and the nuclear condensation and fragmentation characteristic of apoptosis (arrows in Figure S22). Induction of apoptosis was further confirmed by the Annexin V-FITC and propidium iodide (PI) assay using flow cytometry. With this method it was possible to more accurately quantify an induction of apoptosis in cells exposed for 48 h to the complexes (Figure 9).

As expected all complexes at their IC_{50} concentration induce high levels of apoptosis (between 35 % for complex **4** to 18 % for complex **3**) when compared with control cells (4 %) and even when compared to doxorubicin, a common antitumor agent (Figure 9). There is also a slight increase in the levels of necrosis comparing to control cells (Figure 9). As such, these results clearly indicate that the loss of HCT116 cell viability presented in Figure 7 can be due to the induction of apoptosis.

To further comprehend the trigger for complexes-induced cell death via apoptosis the production of reactive oxygen species (ROS) was also evaluated in HCT116 cells exposed to IC_{50} concentrations of the complexes (Figure S23, ESI). It was possible to observe that all compounds can induce the production of ROS (Figure S23, ESI). These results agree with previous published data[30, 123] and the ability of metal complexes to disturb the cellular redox homeostasis of cancer cells as an attractive and promising approach for cancer therapy.[124]

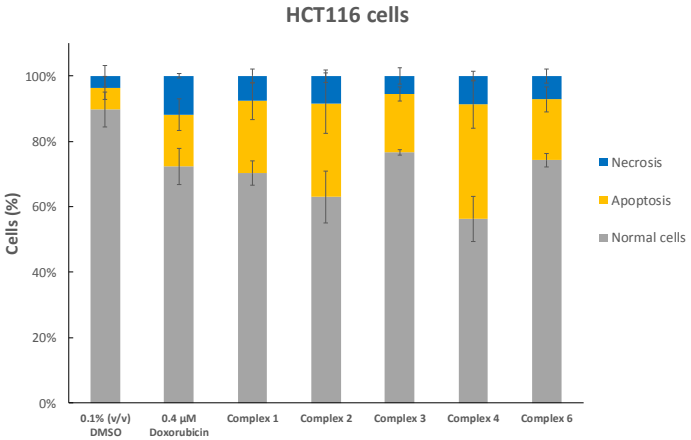

Figure 9 Induction of apoptosis and necrosis in HCT116 cells incubated with IC_{50} concentrations of metallic complexes **1**-**4** and **6** for 48 h measured by the Annexin V-FITC/PI assay. Doxorubicin was used as positive control. The results shown are expressed as the mean ± SD from three independent assays.

Published on 04 April 2018. Downloaded by Fudan University on 04/04/2018 08:52:59.
Dalton Transactions Accepted Manuscript

Please do not adjust margins

View Article Online
DOI: 10.1039/C8DT00558C

Published on 04 April 2018. Downloaded by Fudan University on 04/04/2018 08:52:59.

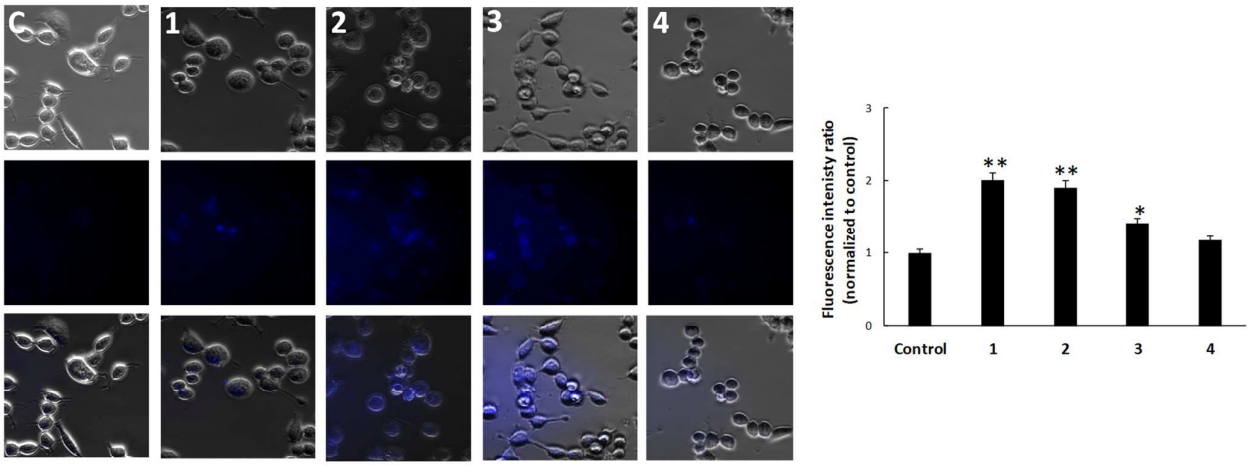

(a) (b)

Figure 10 (a) Representative images of HCT116 cells incubated for 3h in the absence (C, control vehicle 0.1% (v/v) DMSO) or presence of 10x IC_{50} concentrations of complexes **1**-**4**. The lower panel represents the merge of both upper panels to more clearly observe the intracellular fluorescence in HCT116 cells exposed to all complexes. (b) Fluorescence intensity ratio calculated based on the mean of the total HCT116 cell fluorescence after 3h incubation with complexes **1**-**4** normalized to the mean of the total HCT116 cell fluorescence incubated for the same period with the control vehicle 0.1% (v/v) DMSO. The results shown are expressed as the mean ± SD from three independent assays. At least 10 different images per assay were used to calculate the mean of the total fluorescence. **p-value < 0.003 and *p-value < 0.05 relative to control.

To understand if complexes **1–4** do internalize HCT116 cells, fluorescence microscopy was used. As observed in Figure 10 after 3h of incubation of HCT116 cells in the presence or absence of each complex a blue fluorescent staining was co-localized within cells. Despite additional studies might be performed using cell fractioning and ICP-MS analysis, complexes **1**, **4** seems to be more co-localized within the nucleus, with complexes **2** and **3** also distributed through the cell (Figure 10). Interestingly, in complexes **1–4**, the *terpy* framework shows good planarity, which positively correlate with co-localization within the cell. The high levels of fluorescence of complexes **1** and **2** correlates with their higher cytotoxicity compared to complexes **3** and **4** (Figure 10 and Table 5). Considering the redox properties and stability of Au(III) complexes in biological media, we cannot exclude intracellular reduction of Au(III) to Au(I) and it is well known that the effective spin–orbit coupling for Au(I) systems is much larger than that for the Au(III) counterparts, thus resulting in the poor intersystem crossing efficiency for the former.[101]

Conclusions

This work demonstrates spectroscopy, electrochemistry and antiproliferative potential of Au(III), Pt(II) and Cu(II) complexes bearing 4′-substituted 2,2′:6′,2′′-terpyridine ligand, 4′-(4-methoxyphenyl)-2,2′:6′,2′′-terpyridine (**L**^{1}) or 4′-(4-methoxynaphthalen-1-yl)-2,2′:6′,2′′-terpyridine (**L**^{2}). Attention has been paid to investigation of the impact of the substituent introduced into 2,2′:6′,2′′-terpyridine moiety on photophysical and biological properties of the reported transition metal complexes. Remarkably, the complex $[AuCl(L^2)](PF_6)_2$ showed IC_{50} values 300x and 130x higher in normal human fibroblasts compared to the respective values in HCT116 and A2780 cancer cells. What is more, all the complexes display a higher cytotoxic activity in HCT116 cells compared to cisplatin in the same experimental conditions and this loss of cell viability is due to an increase of the apoptosis levels compared to control cells and the induction of ROS. Complexes **1–4** can internalize HCT116 cells and the high cytotoxicity of complexes **1** and **2** compared with complexes **3** and **4** might be correlated with their high internalization levels. The high cytotoxicity of complexes **1**, **2** and **6** (IC_{50} < 1 μM; 30x higher than common antitumor drug cisplatin) in HCT116 colorectal carcinoma cells and their very low cytotoxic activity towards fibroblasts healthy cells is of interest and a positive feature for further developments.

Experimental

Materials

The reagents ($KAuCl_4$, $Pt(PhCN)_2Cl_2$, $CuCl_2{\cdot}2H_2O$, NH_4PF_6, $NaBPh_4$, $Ag(CF_3O_3S)$) used to the synthesis were commercially available and were used without further purification. 2,2':6',2''-terpyridine derivatives were obtained by condensation of 2-acetylpyridine with the corresponding aldehyde (4-methoxybenzaldehyde for **L**^{1} and 4-methoxy-1-naphthaldehyde for **L**^{2})[125–127] according to literature methods.[73, 128, 129] K_2PtCl_4 was prepared as described in the literature.[130] All solvents for synthesis were of reagent grade and they were used as received. For spectroscopy studies spectroscopy grade solvents were used.

Preparation of $[AuCl(L^1)](PF_6)_2{\cdot}CH_3CN$ (1), $[AuCl(L^2)](PF_6)_2$ (2)

$KAuCl_4$ (0.19 g, 0.5 mmol) was refluxed with appropriate ligand **L**^{1} (0.17 g, 0.5 mmol) or **L**^{2} (0.19 g, 0.5 mmol) in a CH_3OH/H_2O mixed solvent (1:4 v/v) (50 cm^3) for ca. 2h. Then an excess of aqueous solution of NH_4PF_6 was added. The mixture was refluxed for another 2 h. The resulting dark orange solution was allowed to evaporate in a hood at room temperature.

Dalton Transactions Accepted Manuscript

This journal is © The Royal Society of Chemistry 20xx

Please do not adjust margins
View Article Online
DOI: 10.1039/C8DT00558C

Published on 04 April 2018. Downloaded by Fudan University on 04/04/2018 08:52:59.

Brown microcrystalline precipitate of **1** and **2** formed after few days was collected by filtration and air-dried. X-ray quality crystals of **1** and **2** were grown by recrystallization from acetonitrile.

[AuCl(L^1)](PF$_6$)$_2$·CH$_3$CN (1): Yield 70%. IR (KBr, cm^{-1}): 1589 (s), 1524 (w), 1488 (m), 1464 (m), 1418 (m), 1367 (m), 1291 (m), 1243 (m), 1190 (m), 1128 (w), 1117 (w), 1041 (m), 1014 (m), 842 (s), 782 (m), 740 (w), 606 (w), 558 (s). ^{1}H NMR (400 MHz, CD_3CN) δ 9.16 (d, *J* = 5.9 Hz, 2H, **H^{A1}**), 8.73 – 8.69 (m, 6H, **H$^{B2, A3, A4}$**), 8.16 (d, *J* = 8.9 Hz, 2H, **H^{C2}**), 8.10 (dt, *J* = 6.2, 2.8 Hz, 2H, **H^{A2}**), 7.28 (d, *J* = 8.8 Hz, 2H, **H^{C3}**), 3.97 (s, 3H, **H^{C5}**). ^{13}C NMR (100 MHz, CD_3CN) δ 165.42 **(C^{C4})**, 159.76 **(C^{B1})**, 159.58 **(C^{B3})**, 153.19 **(C^{A1})**, 153.00 **(C^{A5})**, 147.96 **(C^{A4})**, 132.05 **(C^{A2})**, 131.78 **(C^{C2})**, 129.82 **(C^{A3})**, 126.72 **(C^{C1})**, 124.15 **(C^{B2})**, 116.49 **(C^{C3})**, 56.68 **(C^{C5})**. UV-Vis (CH_3CN, λ_{max}, nm (ε, dm^3·mol^{-1}·cm^{-1})): 264 (18600), 275 (18400), 287 (18400), 296 (25200), 353 (10600), 382 (13300), 419 (17200).

[AuCl(L^2)](PF$_6$)$_2$ (2): Yield 51%. IR (KBr, cm^{-1}): 1607 (m), 1572 (s), 1513 (m), 1488 (m), 1459 (w), 1421 (w), 1360 (m), 1328 (m), 1298 (w), 1240 (m), 1104 (w), 1085 (m), 1041 (w), 902 (w), 840 (s), 779 (m), 739 (w), 717 (w), 621 (w), 558 (s), **^{1}H NMR (400 MHz, CD_3CN) δ** 9.19 (d, *J* = 5.8 Hz, 2H, **H^{A1}**), 8.71 (s, 2H, **H^{B2}**), 8.67 (d, *J* = 7.8 Hz, 2H, **H^{A3}**), 8.60 (d, *J* = 7.9 Hz, 2H, **H^{A4}**), 8.46 – 8.43 (m, 1H, **H^{C9}**), 8.14 – 8.07 (m, 3H, **H^{A2}** and **H^{C6}**), 7.84 (d, *J* = 8.1 Hz, 1H, **H^{C2}**), 7.74 – 7.70 (m, 2H, **H^{C8}** and **H^{C7}**), 7.23 (d, *J* = 8.2 Hz, 1H, **H^{C3}**), 4.15 (s, 3H, **H^{C11}**). **^{13}C NMR (100 MHz, CD_3CN) δ** 161.48 **(C^{B3})**, 159.87 **(C^{C4})**, 159.69 **(C^{A5})**, 153.28 **(C^{A1})**, 153.05 **(C^{B1})**, 147.96 **(C^{A3})**, 132.31 **(C^{C2})**, 132.14 **(C^{A2})**, 131.60 **(C^{C10})**, 130.08 **(C^{A4})**, 129.92 **(C$^{C7 and C8}$)**, 128.71 **(C^{B2})**, 127.76 **(C^{C1})**, 126.58 **(C^{C5})**, 124.82 **(C^{C6})**, 123.80 **(C^{C9})**, 105.35 **(C^{C3})**, 56.97 **(C^{C11})**. UV-Vis (CH_3CN, λ_{max}, nm (ε, dm^3·mol^{-1}·cm^{-1})): 263 (12500), 298 (20700), 347 (9900), 367 (7800), 493 (7600).

Preparation of [PtCl(L^1)](BPh$_4$)·CH$_3$CN (3)

K_2PtCl_4 (0.21 g, 0.5 mmol) was added to DMSO (30 cm^3) at 50 °C. The mixture was stirred up to all amount of precursor dissolved in DMSO. Then a solution of ligand **L^1** (0.17 g, 0.5 mmol) in DMSO (30 cm^3) was added dropwise, and the resulting mixture was stirred for 15 h to yield a deep orange solution. Then an excess of $NaBPh_4$ (as an aqueous/methanol solution) was added dropwise. The resultant orange/brown precipitate of [PtCl(**L^1**)]BPh_4 was isolated by filtration and re-crystallized by vapor diffusion of diethyl ether into an acetonitrile solution of the crude product to afford crystals suitable for X-ray crystal analysis.

[PtCl(L^1)](BPh$_4$)·CH$_3$CN (3): Yield 58%. IR (KBr, cm^{-1}): 1597 (s), 1578 (m), 1520 (m), 1479 (m), 1463 (m), 1413 (m), 1361 (w), 1309 (m), 1260 (m), 1241 (m), 1185 (m), 1032 (m), 1018 (w), 842 (m), 831 (m), 785 (m), 736 (m), 707 (m), 613 (m), 524 (w), 442 (w). ^{1}H NMR (400 MHz, CD_3SOCD_3) δ 8.80 (s, 2H, **H^{B2}**), 8.76 – 8.72 (m, 4H, **H$^{A1 and A4}$**), 8.44 (dt, *J* = 7.9, 0.9 Hz, 2H, **H^{A3}**), 8.14 (d, *J* = 8.8 Hz, 2H, **H^{C2}**), 7.84 (t, *J* = 6.7 Hz, 2H, **H^{A2}**), 7.21 – 7.15 (m, 10H, **H$^{D1 and C3}$**), 6.92 (t, *J* = 7.4 Hz, 8H, **H^{D2}**), 6.78 (t, *J* = 7.2 Hz, 4H, **H^{D3}**), 3.92 (s, 3H, **H^{C5}**). ^{13}C NMR (100 MHz, $(CD_3)_2SO$) δ 164.07 **(C^{D0})**, 162.32 **(C^{C4})**, 158.16 **(C^{A5})**, 154.05 **(C^{B1})**, 152.02 **(C^{B3})**, 151.08 **(C^{A4})**, 142.37 **(C^{A3})**, 135.50 **(C^{D1})**, 129.63 **(C^{C2})**, 129.03 **(C^{A2})**, 126.53 **(C^{C1})**, 125.90 **(C^{A1})**, 125.27 **(C^{D2})**, 121.47 **(C^{D3})**, 120.00 **(C^{B2})**, 114.88 **(C^{C3})**, 55.67 **(C^{C5})**. UV-Vis (CH_3CN, λ_{max}, nm (ε, dm^3·mol^{-1}·cm^{-1})): 270 (8500), 312 (5700), 378 (3800).

Preparation of [PtCl(L^2)](SO$_3$CF$_3$) (4)

A suspension of $[Pt(PhCN)_2Cl_2]$ (0.24 g, 0.5 mmol) in acetonitrile (30 cm^3) was treated with an equimolar amount of $Ag(CF_3O_3S)$ (0.13 g, 0.5 mmol) dissolved in acetonitrile (10 cm^3). The reaction mixture was heated under reflux for 16 h, the AgCl precipitate removed by filtration and one equivalent of ligand added to the filtrate. The reaction mixture was heated in a solvatothermal reactor under atmospheric pressure for an additional 24 h and then gradually cooled by another 24h. The crystals suitable for X-ray analysis were obtained directly from mother liquor.

[PtCl(L^2)](SO$_3$CF$_3$) (4): Yield 68%. IR (KBr, cm^{-1}): 1608 (m), 1575 (s), 1514 (m), 1479 (m), 1458 (m), 1432 (w), 1418 (m), 1390 (w), 1372 (w), 1354 (m), 1324 (m), 1268 (s), 1232 (s), 1160 (s), 1099 (m), 1083 (m), 1059 (w), 1029 (s), 997 (w), 887 (w), 814 (w), 793 (m), 771 (m), 753 (w), 714 (w), 653 (w), 638 (s), 620 (w), 573 (w), 517 (m), 466 (w), 442 (w). ^{1}H NMR (400 MHz, CD_3SOCD_3) δ 8.84 (d, *J* = 5.6 Hz, 2H, **H^{A1}**), 8.82 (s, 2H, **H^{B2}**), 8.70 (d, *J* = 8.0 Hz, 2H, **H^{A4}**), 8.44 (dt, *J* = 7.9, 1.1 Hz, 2H, **H^{A3}**), 8.37 – 8.34 (m, 1H, **H^{C9}**), 8.04 – 8.00 (m, 1H, **H^{C6}**), 7.89 (t, *J* = 6.5 Hz, 2H, **H^{A2}**), 7.73 (d, *J* = 8.0 Hz, 1H, **H^{C2}**), 7.68 – 7.64 (m, 2H, **H$^{C7 and C8}$**), 7.23 (d, *J* = 8.1 Hz, 1H, **H^{C3}**), 4.10 (s, 3H, **H^{C11}**). ^{13}C NMR (100 MHz, $(CD_3)_2SO$) δ 158.41 **(C^{A5})**, 156.57 **(C^{C4})**, 154.07 **(C^{B1})**, 153.91 **(C^{B3})**, 151.11 **(C^{A1})**, 142.57 **(C^{A3})**, 130.62 **(C^{C10})**, 129.11 **(C^{A2})**, 128.97 **(C^{C2})**, 128.05 **(C^{C1})**, 127.29 **(C^{C7})**, 126.20 **(C^{C8})**, 126.00 **(C^{A4})**, 125.51 **(C^{B2})**, 124.97 **(C^{C5})**, 124.62 **(C^{C6})**, 122.22 **(C^{C9})**, 104.24 **(C^{C3})**, 56.12 **(C^{C11})**. UV-Vis (CH_3CN, λ_{max}, nm (ε, dm^3·mol^{-1}·cm^{-1})): 253 (24000), 283 (26700), 302 (17100), 315 (16200), 338 (13300), 423 (8500).

Preparation of [CuCl$_2$(L^1)] (5) and [CuCl$_2$(L^2)]·(CH$_3$CN) (6)

Compounds **5** and **6** were prepared according to the method given in the literature.[28] $CuCl_2·2H_2O$ (0.08 g, 1 mmol) dissolved in methanol (10 cm^3) was added dropwise to a hot methanolic solution of ligand **L^1** (0.17 g, 0.5 mmol) or **L^2** (0.19 g, 0.5 mmol). The resulting solution was stirred at room temperature for 2 h and then allowed to evaporate in a hood at room temperature. After a few days green precipitate was isolated by filtration and re-crystallized from acetonitrile.

[CuCl$_2$(L^2)] (5): Yield 74%. IR (KBr, cm^{-1}): 1597 (s), 1579 (m), 1555 (m), 1555 (m), 1524 (s), 1476 (s), 1436 (m), 1412 (m), 1369 (w), 1313 (w), 1286 (m), 1243 (s), 1191 (s), 1066 (m), 1041 (w), 1021 (m), 1009 (m), 895 (w), 835 (m), 792 (s), 750 (m), 725 (w), 657 (w), 646 (m), 585 (m), 516 (w), 417 (w). UV-Vis (CH_3CN, λ_{max}, nm (ε, dm^3·mol^{-1}·cm^{-1})): 226 (19700), 257 (21900), 265 (12900), 288 (11900), 339 (13300), 707 (1300).

[CuCl$_2$(L^2)]·(CH$_3$CN) (6): Yield 90%. IR (KBr, cm^{-1}): 1607 (s), 1579 (s), 1551 (m), 1514 (s), 1475 (s), 1430 (m), 1417 (m), 1394 (m), 1362 (m), 1325 (m), 1292 (m), 1246 (m), 1235 (s), 1161 (m), 1115 (m), 1092 (s), 1048 (m), 1037 (m), 1019 (m), 999 (w), 955 (m), 882 (w), 843 (w), 802 (m), 788 (m), 766 (m), 742 (m), 713 (w), 662 (m), 655 (m), 645 (m), 611 (m), 516 (w), 417 (w). UV-Vis (CH_3CN, λ_{max}, nm (ε, dm^3·mol^{-1}·cm^{-1})): 257 (21100), 289 (16000), 324 (16600), 369 (8500), 761 (1300).

Dalton Transactions Accepted Manuscript

Please do not adjust margins

View Article Online
DOI: 10.1039/C8DT00558C

Published on 04 April 2018. Downloaded by Fudan University on 04/04/2018 08:52:59.

Physical measurements

IR spectra were recorded on a Nicolet iS5 spectrophotometer in the spectral range 4000–400 cm^{-1} with the samples in form of KBr pellets. The NMR spectra were recorded on a Bruker Avance 400 MHz spectrometer by using dimethyl sulfoxide-d_6 ($(CD_3)_2SO$) or acetonitrile-d_3 (CD_3CN) as solvent. Chemical shifts (δ) are reported in parts per million (ppm) and referenced to residual solvent peak ($(CD_3)_2SO$: ^1H δ = 2.50 ppm, ^{13}C δ = 39.52 ppm, CD_3CN: ^1H δ = 1.94 ppm, ^{13}C δ = 118.26 ppm). Coupling constants (J) are reported in Hz. The peak multiplicity is designated by a singlet (s), doublet (d), triplet (t), doublet of triplets (dt), and multiplet (m). The labels A, B and C refer to the central pyridine ring, peripheral pyridine ring and substituent ring/rings, respectively. Homonuclear correlation spectroscopy was performed using 2D COSY experiments, while heteronuclear correlation spectroscopy was done on the basis of HMQC or HMBC (long-range) experiments.

The electronic spectra were measured on spectrophotometer Nicolet Evolution 220 in the range 240–1000 nm in acetonitrile ($c = 5 \cdot 10^{-5}$ M). UV-Vis spectroscopy was also used to study of stability of the gold(III) complexes in acetonitrile, phosphate buffered saline (PBS, pH 7.4, 130 mM NaCl) and PBS buffer in the presence of equimolar amount of sodium ascorbate (SA) or reduced glutathione (GSH). The concentration of the gold(III) complexes in the final samples was 5 □ 10^{-5} M. For the stability in PBS buffer, Au(IIII) complexes were dissolved in a minimum amount of DMSO, and then diluted in phosphate buffered saline to a final concentration of $5 \cdot 10^{-5}$ M. The resulting solutions were monitored by collecting spectrum once every four hours over 24 h at room temperature.

The photoluminescence spectra (PL) were undertaken on the FLS-980 spectrophotometer equipped with a 450 W Xe lamp and a high-gain photomultiplier PMT + 500 nm (Hamamatsu, R928P) detector. The spectra were prepared in acetonitrile solutions (5 □ 10^{-4} M) at ambient condition as well as in methanol:ethanol (1:4 v/v) frozen-glass matrix at temperature of liquid nitrogen with Dewar assemble. The quantum yields were examined in acetonitrile solutions using integrating sphere direct method. The solvent and Spectralon® reference standards were used as blanks, respectively in the case of diluted solutions and powder samples. The complexes were excited with wavelength in each case corresponding to the obtained excitation bands. The FLS-980 software was used to designate the quantum yield values. The time-resolved measurement was carried out using the time correlated single photon counting methods (TCSPC) on the FLS-980 spectrophotometer. Excitation wavelength was obtained using the set of picosecond pulsed diodes (EPLED–280 nm, EPL–375 nm, EPL-405 nm) or microsecond lamp as light sources and high-gain photomultiplier PMT+500 nm (Hamamatsu, R928P) in cooled housing as a detector. The system was aligned at the emission wavelengths. Additionally, for the analysis of a fluorescence decay, an instrument response function (IRF) was obtained. The IRF contains the information about the time response of the overall optical and electronic system. The IRF was designated using ludox solution as a standard at excitation wavelengths. The decay curves were bi-exponentially fitted using reconvolution/tail fit analysis included in FLS-980 software.

Cyclic voltammetry (CV) measurements were carried out on the Autolab potentiostat (Eco Chemie). A three-electrode one-compartment cell was used to contain the solution of complexes and supporting electrolyte in CH_3CN. Deaeration of the solution was achieved by argon bubbling through the solution for about 10 min before measurement. The complexes and supporting electrolyte ($n\text{-}Bu_4NPF_6$) concentrations were equal to 1 □ 10^{-6} M and 0.1 M, respectively. The scan rate was equal to 0.1 V/s. A glassy carbon disk working electrode (3 mm diam.), and an Ag/Ag^+ reference electrodes were used. All electrochemical experiments were carried out under ambient conditions.

Crystal structure determination and refinement

The X-ray diffraction data was collected on single crystals by means of an Oxford Diffraction four-circle diffractometer Gemini A Ultra with Atlas CCD detector using graphite monochromated MoKα radiation (λ = 0.71073 Å) at room temperature. Diffraction data collection, cell refinement and data reduction were performed using the CrysAlis^{Pro} software.[131] The structures were solved by the direct methods using SHELXS and refined by full-matrix least-squares on F^2 using SHELXL-2014.[132] All the non-hydrogen atoms were refined anisotropically, and hydrogen atoms were placed in calculated positions refined using idealized geometries (riding model) and assigned fixed isotropic displacement parameters, d(C–H) = 0.93 Å, U_{iso}(H) = 1.2 U_{eq}(C) (for aromatic) and d(C–H) = 0.96 Å, U_{iso}(H) = 1.5 U_{eq}(C) (for methyl and water). The methyl groups were allowed to rotate about their local threefold axis. Details of the crystallographic data collection, structural determination, and refinement for **1**–**5** are given in Table 6. CCDC 1823066, 1823065, 1509477, 1823063 and 1823064 contain the supplementary crystallographic data for **1**–**5**. The data can be obtained free of charge from The Cambridge Crystallographic Data Centre at www.ccdc.cam.ac.uk/getstructures.

Powder X-ray diffraction (PXRD) measurements were performed on a PANalytical Empyrean X-ray diffractometer using Cu−Kα radiation (λ = 1.5418 Å), in which the X-ray tube was operated at 40 kV and 30 mA ranging from 5 to 90°. The experimental and calculated powder X-ray diffraction (PXRD) patterns for all the complexes show a great coincidence of the positions of all peaks expected, each pattern confirming that the obtained structure from the single crystal is equal to the one of the bulk (Figure S8, ESI).

Biological assays

Cell culture

Human colorectal (HCT116) and ovarian carcinoma (A2780) cell lines were grown in Dulbecco's modified Eagle's medium (DMEM) (Invitrogen Corp., Grand Island, NY, USA) supplemented with 10% foetal bovine serum and 1% antibiotic/antimycotic solution (Invitrogen Corp.) and

Dalton Transactions Accepted Manuscript

This journal is © The Royal Society of Chemistry 20xx

Please do not adjust margins
View Article Online
DOI: 10.1039/C8DT00558C

Table 6. Crystal data and structure refinement.

	1	2	3	4	6
Empirical formula	$C_{24}H_{20}AuClF_{12}N_4OP_2$	$C_{26}H_{19}AuClF_{12}N_3OP_2$	$C_{48}H_{40}PtClN_4OB$	$C_{27}H_{19}PtClF_3N_3O_4S$	$C_{28}H_{22}Cl_2CuN_4O$
Formula weight	902.80	911.80	930.19	769.05	564.93
Temperature [K]	295.0(2)	295.0(2)	295.0(2)	295.0(2)	295.0(2)
Wavelength [Å]	0.71073	0.71073	0.71073	0.71073	0.71073
Crystal system	monoclinic	monoclinic	triclinic	monoclinic	triclinic
Space group	*P2₁/c*	*P2₁/c*	*P-1*	*P2₁/c*	*P-1*
Unit cell dimensions [Å, °]	a = 15.2102(8)	a = 8.0750(3)	a = 7.8085(3)	a = 11.8647(7)	a = 7.2767(3)
	b = 12.3174(5)	b = 21.7655(9)	b = 15.6671(7)	b = 14.5225(8)	b = 12.0071(7)
	c = 17.3958(6)	c = 17.4149(6)	c = 17.1368(5)	c = 15.1167(7)	c = 14.7218(6)
	α = 90	α = 90	α = 77.338(3)	α = 90	α = 83.765(4)
	β = 109.289(5)	β = 93.847(3)	β = 89.736(3)	β = 94.526(5)	β = 88.612(3)
	γ = 90	γ = 90	γ = 76.579(4)	γ = 90	γ = 81.976(4)
Volume [Å³]	3076.2(2)	3053.9(2)	1987.24(14)	2596.6(2)	1266.09(11)
Z	4	4	2	4	2
Density (calculated) [mg/m³]	1.949	1.983	1.555	1.967	1.482
Absorption coefficient [mm⁻¹]	5.073	5.111	3.640	5.650	1.103
F(000)	1736	1752	928	1488	578
Crystal size [mm]	0.19 x 0.10 x 0.07	0.25 x 0.10 x 0.06	0.30 x 0.08 x 0.06	0.08 x 0.07 x 0.04	0.12 x 0.10 x 0.07
θ range for data collection [°]	3.31 to 29.47	3.42 to 29.39	3.35 to 29.51	3.29 to 29.34	3.31 to 29.42
Index ranges	-18 ≤ h ≤ 20	-10 ≤ h ≤ 10	-10 ≤ h ≤ 10	-16 ≤ h ≤ 11	-8 ≤ h ≤ 9
	-17 ≤ k ≤ 11	-21 ≤ k ≤ 29	-19 ≤ k ≤ 21	-19 ≤ k ≤ 17	-14 ≤ k ≤ 16
	-23 ≤ l ≤22	-22 ≤ l ≤ 22	-23 ≤ l ≤ 22	-20 ≤ l ≤ 18	-19 ≤ l ≤ 18
Reflections collected	17342	19911	23654	14217	11592
Independent reflections	5433 (R_{int} = 0.035)	7412 (R_{int} = 0.042)	9487 (R_{int} = 0.050)	6152 (R_{int} = 0.084)	5914 (R_{int} = 0.0395)
Completeness to 2θ=50° [%]	99.7	99.7	99.8	99.4	99.8
Max. and min. transmission	0.502 and 1.000	0.575 and 1.000	0.375 and 1.000	0.0271 and 1.000	0.763 and 1.000
Data / restraints / parameters	5433 / 0 / 408	7412/ 0 / 416	9487 / 0 / 544	6152 / 0 / 362	5914 / 0 / 327
Goodness-of-fit on F²	1.011	1.029	1.016	0.900	1.049
Final R indices [I>2σ(I)]	R1 = 0.0494	R1 = 0.0515	R1 = 0.0459	R1 = 0.0506	R1 = 0.0497
	wR2 = 0.1189	wR2 = 0.1091	wR2 = 0.0949	wR2 = 0.0717	wR2 = 0.0911
R indices (all data)	R1 = 0.0811	R1 = 0.0871	R1 = 0.0664	R1 = 0.1173	R1 = 0.0864
	wR2 = 0.1359	wR2 = 0.1248	wR2 = 0.1061	wR2 = 0.0875	wR2 = 0.1074
Largest diff. peak and hole [e Å⁻³]	1.17 and -1.15	0.98 and -0.76	1.96 and -1.37	1.67 and -1.29	0.49 and -0.46
CCDC number	1823066	1823065	1509477	1823063	1823464

maintained at 37 °C in a humidified atmosphere of 5% (v/v) CO_2 Normal Human fibroblasts were grown in the same conditions, supplemented with 1% MEM non-essential amino acids (Invitrogen Corp.). All cell lines were purchased from ATCC (www.atcc.org) with the exception of A2780 that was purchased from Sigma-Aldrich (www. sigmaaldrich.com).

Complexes exposure for dose-response curves

Cells were plated at 5000 cells/well in 96-well plates. Media was removed 24 h after platting and replaced with fresh media containing: 0.1–150 µM of complexes **1–6** or Ligands $\mathbf{L^1}$ and $\mathbf{L^2}$ or 0.1% (v/v) DMSO (vehicle control). All the previous solutions were prepared from concentrated stock solutions (in DMSO) of the complexes **1–5** and ligands.

Viability assays

After 48 h of cell incubation in the presence or absence of complexes **1–6**, ligands $\mathbf{L^1}$ and $\mathbf{L^2}$ or vehicle control, cell viability was evaluated with CellTiter 96® AQueous Non-Radioactive Cell Proliferation Assay (Promega, Madison, WI, USA), using 3-(4,5-dimethylthiazol-2-yl)-5-(3-carboxymethoxyphenyl)-2-(4-sulfophenyl)-2H-tetrazolium, inner salt (MTS) as previously described.[8] In brief, this is a homogeneous, colorimetric method for determining the number of viable cells in proliferation, cytotoxicity or chemo-sensitivity assays. The CellTiter 96® AQueous Assay is composed of solutions of MTS and an electron coupling reagent (phenazinemethosulfate, PMS). MTS is bio-reduced by cells into a formazan product that is soluble in tissue culture medium. The absorbance of the formazan product at 490 nm can be measured directly from 96-well assay plates without additional processing. The conversion of MTS into the aqueous soluble formazan product is accomplished by dehydrogenase enzymes found in metabolically active cells. The quantity of formazan product was measured in a Bio-Rad microplate reader Model 680 (Bio-Rad, Hercules, CA, USA) at 490 nm, as absorbance is directly proportional to the number of viable cells in culture. The interference in the MTS assay by ligands or metal complexes per se was also evaluated by incubating the molecules in DMEM medium with the MTS reagent and without cells. This value was subtracted from the absorbance in vehicle control cells. HCT116 and A2780 Cell viability was also evaluated by trypan blue exclusion method using 0.5x IC_{50}, IC_{50} and 2x IC_{50} concentrations of each complex or ligand. After

Published on 04 April 2018. Downloaded by Fudan University on 04/04/2018 08:52:59.
Dalton Transactions Accepted Manuscript
This journal is © The Royal Society of Chemistry 20xx

Please do not adjust margins

View Article Online
DOI: 10.1039/C8DT00558C

Published on 04 April 2018. Downloaded by Fudan University on 04/04/2018 08:52:59.

48 h incubation, cells were trypsinised and stained with 0.2% (v/v) trypan blue and counted in a Neubauer improved haemocytometer (Marienfeld Superior).

Assessment of apoptosis through Hoechst 33258 staining

HCT116 cells grown as described above were plated at 7500 cells/mL and incubated for 48 h in culture medium containing the complexes **1**–4, **6** (at their IC_{50}) or 0.1% (v/v) DMSO (vehicle control). Hoechst staining (excitation and fluorescence emission 352 and 461 nm, respectively) was used to detect apoptotic nuclei as previously described.[8] Briefly, medium was removed, cells were washed with phosphate-buffered saline 1X (PBS) (Invitrogen), fixed with 4% (v/v) paraformaldehyde in PBS 1X (10 min in the dark) and incubated with Hoechst dye 33258 (Sigma, Missouri, USA; 5 μg/mL in PBS 1X) for another 10 min. After washed with PBS 1X, cells were mounted using 20 μL of PBS:glicerol (3:1; v/v) solution. Fluorescent nuclei were sort out per the chromatin condensation degree and characteristics. Normal nuclei showed non-condensed chromatin uniformly distributed over the entire nucleus. Apoptotic nuclei showed condensate or fragmented chromatin. Some cells formed apoptotic bodies. Plates were photographed in an AXIO Scope (Carl Zeiss, Oberkochen Germany), and three random microscopic fields per sample with ca. 50 nuclei were counted. Mean values were expressed as the percentage of apoptotic nuclei.[8]

Assessment of apoptosis through Annexin V-FITC/PI Dead Cell Apoptosis assay

HCT116 cells were grown as previously described and plated at 7500 cell/mL in 6-well plates and incubated for 48 h with IC_{50} concentrations of each complex or ligand. The Annexin V-FITC/PI Dead Cell Apoptosis kit (ThermoFisher Scientific) was then used according to the manufacturer's instructions. Briefly, cells were detached with trypsin, washed thrice with PBS and incubated with Annexin V conjugated with FITC fluorophore and/or 10 μg/mL propidium iodide (PI). After an incubation of 15 min. cells were analysed in an Attune acoustic focusing cytometer (ThermoFisher Scientific) using the Attune Cytometric Software, vs 2.1. Doxorobucin, a common antitumor drug was used as positive control (0.4 μM). Information was presented as the average of cells (in percentage) in apoptosis, necrosis or in a normal physiological state.

Production of Reactive Oxygen Species (ROS) in HCT116 cells

HCT116 cells were incubated with IC_{50} concentrations of each complex or ligand for 48 h. Cells were then collected and washed twice in PBS and then incubated for 30 min at 37 °C with 10 μM 2',7'-dichlorodihydrofluorescein diacetate (H_2DCF-DA) (ThermoFisher Scientific). Upon internalization in cells, cellular esterases remove acetate groups and in the presence of ROS, the dye is oxidized, with an increase of the fluorescence of the compound. Cells were then analysed in an Attune acoustic focusing cytometer (ThermoFisher Scientific) with the corresponding software (Attune Cytometric Software, vs 2.1). Hydrogen Peroxide (H_2O_2) was used as positive control (25 μM). Information was presented as the mean fluorescence intensity of each sample normalized to the fluorescence intensity of control cells exposed to 0.1% (v/v) DMSO (vehicle control).

Internalization of complexes 1-4 by fluorescence microscopy

HCT116 cells were seeded at a density of 200000 cells per ml in 96-well plates and incubated for 3 h in supplemented DMEM culture medium containing complexes **1**–**4** at 10x the respective IC_{50} or 0.1% (v/v) DMSO (vehicle control). The culture medium was removed, and cells were washed with phosphate-buffered saline 1x (PBS) (Invitrogen) and observed in a Ti-U Eclipse inverted fluorescence microscope (Nikon, Tokyo, Japan) with a DAPI fluorescence filter cube with an excitation filter of 340–380 nm, a dichroic mirror at 400 nm and a barrier filter at 435–485 nm (Nikon) and images captured using NIS Elements Basic software (Nikon). The corrected total cell fluorescence was calculated by measuring the intensity of cell fluorescence and subtracting the background fluorescence. At least 10 different random microscopic fields were observed for each condition/complex. Acquisition times were set equal in all fluorescence images. Mean values were expressed as fluorescence ratio (complexes versus control). Image measurements were made with ImageJ v1.51s.

Statistical analysis

All data were expressed as mean ± SEM from at least three independent experiments. Statistical significance was evaluated using the Student's t-test; $p < 0.05$ was considered statistically significant. Statistical analysis was performed using GraphPad Prism v6.01 (GraphPad Software, La Jolla, CA, USA).

Computational details

The calculations have been performed using the GAUSSIAN-09 program package.[93] The geometries of the singlet ground state (S_0) of **1-4** were fully optimized without any symmetry restrictions at the DFT level with the PBE1PBE hybrid exchange-correlation functional[133–135]. The calculations were performed using the def2-TZVP basis set for carbon, oxygen, nitrogen, chlorine and hydrogen atoms, while for gold Stuttgart Relativistic, Small Core ECP Basis Set with corresponding pseudopotentials.[136–139] The starting point for geometry optimization was taken from X-ray structure, and all the subsequent calculations were performed based on the optimized geometries. Vibrational frequencies were calculated on the basis of the optimized geometry to verify that each of the geometries is a minimum on the potential energy surface. Furthermore, on the basis of the optimized ground state geometries, the absorption properties in acetonitrile (CH_3CN) media were calculated by TD-DFT at the PBE1PBE hybrid functional level and with the polarized continuum model (PCM).[140-142] The predicted bond lengths and angles for the ground state are within the range of error expected for DFT calculations and the general trends observed in the experimental data are well reproduced in the calculations, providing confidence on the reliability of the chosen method to reproduce the geometry of the studied complex.

Acknowledgements

Dalton Transactions Accepted Manuscript

This journal is © The Royal Society of Chemistry 20xx

Please do not adjust margins
View Article Online
DOI: 10.1039/C8DT00558C

Published on 04 April 2018. Downloaded by Fudan University on 04/04/2018 08:52:59.

This work was supported by the National Science Centre of Poland under grant MINIATURA 1 (2017/01/X/ST5/00026), the Unidade de Ciências Biomoleculares Aplicadas-UCIBIO, which is financed by national funds from the FCT/MEC (UID/Multi/04378/2013 and PTDC/CVT-EPI/6685/2014) and co-financed by the ERDF under the PT2020 Partnership Agreement (POCI-01-0145-FEDER-007728). We also acknowledge PV Baptista for microplate reader access.

References

1 A. Winter, G. R. Newkome, and U. S. Schubert, *ChemCatChem*, 2011, **3**, 1384–1406;
2 L. Cristian, S. Nica, O. D. Pavel, C. Mihailciuc, V. Almasan, S. M. Coman, C. Hardacre and V. I. Parvulescu, *Catal. Sci. Technol.*, 2013, **3**, 2646–2653;
3 H. Yamazaki, T. Ueno, K. Aiso, M. Hirahara, T. Aoki, T. Nagata, S. Igarashi and M. Yagi, *Polyhedron*, 2013, **52**, 455–460;
4 Z. Ma, L. Wei, E. C. B. A. Alegria, L. M. D. R. S. Martins, M. F. C. G. da Silva and A. J. L. Pombeiro, *Dalton Trans.*, 2014, **43,** 4048–4058;
5 A. Draksharapu, A. J. Boersma, M. Leising, A. Meetsma, W. R. Browne and G. Roelfes, *Dalton Trans.*, 2015, **44,** 3647–3655;
6 L. Yan, R. Zong and Y. Pushkar, *J. Catal.*, 2015, **330**, 255–260;
7 G. Zhang, E. Liu, C. Yang, L. Li, J. A. Golen and A. L. Rheingold, *Eur. J. Inorg. Chem.*, 2015, **2015**, 939–947;
8 K. Czerwińska, B. Machura, S. Kula, S. Krompiec, K. Erfurt, C. Rodrigues, A. Fernandes, L. S. Shul'pina, N. S. Ikonnikov and G. B. Shul'pin, *Dalton Trans.*, 2017, **46**, 9591–9604;
9 J. A. G. Williams, S. Develay, D. L. Rochester and L. Murphy, *Coord. Chem. Rev.*, 2008, **252**, 2596–2611;
10 D. A. K. Vezzu, J. C. Deaton, J. S. Jones, L. Bartolotti, C. F. Harris, A. P. Marchetti, M. Kondakova, R. D. Pike and S. Huo, *Inorg. Chem.*, 2010, **49**, 5107–5119;
11 E. Turner, N. Bakken and J. Li, *Inorg. Chem.,* 2013, **52**, 7344–7351;
12 A. Maroń, A. Szlapa, K. Czerwińska, J. G. Małecki, S. Krompiec and B. Machura, *CrystEngComm*, 2016, **18**, 5528–5536
13 T. Klemens, A. Świtlicka-Olszewska, B. Machura, M. Grucela, E. Schab-Balcerzak, K. Smolarek, S. Maćkowski, A. Szlapa, S. Kula, S. Krompiec, P. Lodowski and A. Chrobok, *Dalton Trans.*, 2016, **45**, 1746–1762;
14 S. Martinez-Vargas, J. Valdés-Martínez and A. I. Martinez, *J. Mol. Struct.,* 2011, **1006**, 425–433;
15 C. M. A. Ollagnier, D. Nolan, C. M. Fitchett and S. M. Draper, *Supramol. Chem.*, 2012, **24**, 563–571;
16 E. A. Hassan, M. L. Hassan, C. N. Moorefield and G. R. Newkome, *Carbohyd. Polym.,* 2015, **116**, 2–8;
17 J. R. Thompson, K. A. S. Goodman-Rendall and D. B. Leznoff, *Polyhedron*, 2016, **108**, 93–99;
18 C. Bai, B. Xu, H.-M. Hu, M.-L. Yang and G. Xue, *Polyhedron*, 2017, **124**, 1–11;
19 G. Lowe, A. S. Droz, T. Vilaivan, G. W. Weaver, J. J. Park, J. M. Pratt, L. Tweedale and L. R. Kelland, *J. Med. Chem*., 1999, **42**, 3167–3174;
20 I. Ott and R. Gust, *Arch. Pharm. Chem. Life Sci.,* 2007, **340**, 117–126;
21 M. N. Patel, H. N. Joshi and C. R. Patel, *Polyhedron*, 2012, **40**, 159–167;
22 V. M. Manikandamathavan, V. Rajapandian, A. J. Freddy, T. Weyhermüller, V. Subramanian and B. U. Nair, *Eur. J. Med. Chem.*, 2012, **57**, 449–458;
23 M. N. Patel, H. N. Joshi and C. R. Patel, *J. Organomet. Chem.*, 2012, **701**, 8–16;
24 W. Chu, Y. Wang, S. Liu, X. Yang and J. Zhang; *Bioorg. Med. Chem. Lett.*, 2013, **23**, 5187–5191;
25 S. Wang, W. Chu, Y. Wang, S. Liu, J. Zhang, S. Li, H. Wei, G. Zhou and X. Qin, *Appl. Organomet. Chem.*, 2013, **27**, 373–379;
26 G.-Y. Li, K.-J. Du, J.-Q. Wang, J.-W. Liang, J.-F. Kou, X.-J. Hou, L.-N. Ji and H. Chao, *J. Inorg. Biochem.*, 2013, **119**, 43–53;
27 N. Cutillas, G. S. Yellol, C. de Haro, C. Vicente, V. Rodriguez and J. Ruiz, *Coord. Chem. Rev.*, 2013, **257**, 2784–2797;
28 J.-W. Liang, Y. Wang, K.-J. Du, G.-Y. Li, R.-L. Guan, L.-N. Ji and H. Chao, *J. Inorg. Biochem*., 2014, **141**, 17–27;
29 F. Trudu, F. Amato, P. Vaňhara, T. Pivetta, E. M. Peña-Méndez and J. Havel, *J. Appl. Biomed*., 2015, **13**, 79–103;
30 A. S. Mendo, S. Figueiredo, C. Roma-Rodrigues, P. A. Videira, Z. Ma, M. Diniz, M. Larguinho, P. M. Costa, J. C. Lima, A. J. L. Pombeiro, P. V. Baptista and A. R. Fernandes, *J. Biol. Inorg. Chem.*, 2015, **20**, 935–948;
31 D. Mahendiran, P. Gurumoorthy, K. Gunasekaran, R. S. Kumar and A. K. Rahiman, *New J. Chem.*, 2015, **39**, 7895–7911
32 S. Medici, M. Peana, V. M. Nurchi, J. I. Lachowicz, G. Crisponi and M. A. Zoroddu, *Coord. Chem. Rev.*, 2015, **284**, 329–350;
33 G. Zhang, J. Tan, Y. Z. Zhang, C. Ta, S. Sanchez, S.-Y. Cheng, J. A. Golen and A. L. Rheingold, *Inorganica Chim. Acta*, 2015, **435**, 147–152;
34 Z. Ma, B. Zhang, M. F. C. Guedes da Silva, J. Silva, A. S. Mendo, P. V. Baptista, A. R. Fernandes and A. J. L. Pombeiro, *Dalton Trans.*, 2016, **45**, 5339–5355;
35 W. Liu and R. Gust, *Coord. Chem. Rev.*, 2016, **329**, 191–213;
36 K. Czerwińska, M. Golec, M. Skonieczna, J. Palion-Gazda, D. Zygadło, A. Szlapa-Kula, S. Krompiec, B. Machura and A. Szurko, *Dalton Trans.*, 2017, **46**, 3381–3392;
37 M. M. Milutinović, A. Rilak, I. Bratsos, O. Klisurić and Ž. D. Bugarčić, *J. Inorg. Biochem.,* 2017, **169**, 1–12;
38 D.-Y. Zhang, Y. Nie, H. Sang, J.-J. Suo, Z.-J. Li, W. Gu, J.-L. Tian, X. Liu and S.-P. Yan, *Inorg. Chim. Acta*, 2017, **457**, 7–18;
39 S. Roy, S. Saha, R. Majumdar, R. R. Dighe and A. R. Chakravarty, *Polyhedron*, **29**, 2010, 2787–2794;
40 K. Suntharalingam, D. J. Hunt, A. A. Duarte, A. J. P. White, D. J. Mann and R. Vilar, *Chem. Eur. J.*, 2012, **18**, 15133–15141;
41 V. M. Manikandamathavan and B. U. Nair*, Eur. J. Med. Chem*., 2013, **68**, 244–252;
42 X.-F. Zhao, Y. Ouyang, Y.-Z. Liu, Q.-J. Su, H. Tian, C.-Z. Xie and J.-Y. Xu, *New J. Chem.,* 2014, **38**, 955–965;
43 M.-J. Li, T.-Y. Lan, X.-H. Cao, H.-H. Yang, Y. Shi, C. Yi and G.-N. Chen, *Dalton Trans.*, 2014, **43**, 2789–2798;
44 J. Grau, R. F. Brissos, J. Salinas-Uber, A. B. Caballero, A. Caubet, O. Roubeau, L. Korrodi-Gregório, R. Pérez-Tomás and P. Gamez, *Dalton Trans*., 2015, **44**, 16061–16072;
45 M. Wehbe, A. W. Y. Leung, M. J. Abrams, C. Orvig and M. B. Ballya, *Dalton Trans.,* 2017, **46**, 10758–10773;
46 K. Tummalapalli, C.S. Vasavi, P. Munusami, M. Pathak and M. M. Balamurali, *Int. J. Biol. Macromol.,* **95**, 1254–1266;
47 H. Bertrand, D. Monchaud, A. De Cian, R. Guillot, J.-L. Mergny and M.-P. Teulade-Fichou, *Org. Biomol. Chem.*, 2007, **5**, 2555–2559;
48 K. Suntharalingam, A. J. P. White and R. Vilar, *Inorg. Chem*., 2009, **48**, 9427–9435;
49 C. Wei, L. Ren and N. Gao, *Int. J. Biol. Macromol*., 2013, **57**, 1–8;
50 V. S. Stafford, K. Suntharalingam, A. Shivalingam, A. J. P. White, D. J. Mann and R. Vilar, *Dalton Trans.,* 2015, **44**, 3686–3700;
51 Z. Ou, Y. Qian, Y. Gao, Y. Wang, G. Yang, Y. Li, K. Jiang and X. Wang, *RSC Adv.*, 2016, **6**, 36923–36931;
52 S. Gama, I. Rodrigues, F. Mendes, I. C. Santos, E. Gabano, B. Klejevskaja, J. Gonzalez-Garcia, M. Ravera, R. Vilar and A. Paulo, *J. Inorg. Biochem*., 2016, **160**, 275–286;
53 E. Morel, F. Poyer, L. Vaslin, S. Bombard and M.-P. Teulade-Fichou, *Inorg. Chim. Acta*, 2016, **452**, 152–158;

Dalton Transactions Accepted Manuscript

Please do not adjust margins

View Article Online
DOI: 10.1039/C8DT00558C

54 Q. Cao, Y. Li, E. Freisinger, P. Z. Qin, R. K. O. Sigel and Z.-W. Mao, *Inorg. Chem. Front*., 2017, **4**, 10–32;
55 V. Milacic and Q. P. Dou, *Coord. Chem. Rev.,* 2009, **253**, 1649–1660
56 R. J. Puddephatt, *The Chemistry of Gold*, Elsevier, Amsterdam, 1978;
57 M. Dinger and W. Henderson, *J. Organomet. Chem.*, 1998, **560**, 233–243;
58 L. Ronconi, C. Marzano, P. Zanello, M. Corsini, G. Miolo, C. Macca, A. Trevisan and D. Fregona, *J. Med. Chem*., 2006, **49**, 1648–1657;
59 G. Annibale, M. Brandolisio and B. Pitteri, *Polyhedron*, 1995, **14**, 451–453;
60 S.C. Dhara, *Indian J. Chem*, 1970, **8**, 193–194;
61 A. M. Heyns and G. W. van Schalkwyk, *Spectrochim. Acta A*, 1973, 29, 1163–1176;
62 G. A. Lawrance, *Chem. Rev.,* 1986, **86**, 17–33;
63 L. Yang, D. R. Powell and R. P. Houser, *Dalton Trans*., 2007, 955–964;
64 A. Okuniewski, D. Rosiak, J. Chojnacki and B. Becker, *Polyhedron*, 2015, **90**, 47–57;
65 A. W. Addison, T. N. Rao, J. Reedijk, J. van Rijn and G. C. Verschoor, *J. Chem. Soc., Dalton Trans.,* 1984, 1349–1356;
66 H. A. Jahn and E. Teller, *Proc. R. Soc. A.,* 1937, **161**, 220–235;
67 M. A. Spackman and J. J. McKinnon, *CrystEngComm*, 2002, **4**, 378–392;
68 M. A. Spackman and D. Jayatilaka, *CrystEngComm*, 2009, **11**, 19–32;
69 S. K. Wolff, D. J. Grimwood, J. J. McKinnon, M. J. Turner, D. Jayatilaka and M. A. Spackman, Crystal Explorer (Version 3.1), University of Western Australia, 2012;
70 C. R. Groom, I. J. Bruno, M. P. Lightfoot and S. C. Ward, Acta Crystallogr., Sect. B: Struct. Sci., 2016, 72, 171–179.
71 V. M. Miskowski and V. H. Houlding, *Inorg. Chem*., 1991, **30**, 4446–4452;
72 A. Poater, S. Moradell, E. Pinilla, J. Poater, M. Solà, M. Á. Martínez and A. Llobet, *Dalton Trans.,* 2006, 1188–1196;
73 A. Maroń, A. Szlapa, T. Klemens, S. Kula, B. Machura, S. Krompiec, J. G. Małecki, A. Świtlicka-Olszewska, K. Erfurt and A. Chrobok, *Org. Biomol. Chem*., 2016, **14**, 3793–3808;
74 M. A. Mansour, R. J. Lachicotte, H. J. Gysling and R. Eisenberg, *Inorg. Chem.*, 1998, **37**, 4625–4632
75 S.-W. Lai, M. C. W. Chan, K.-K. Cheung and C.-M. Che, *Inorg. Chem.* 1999, **38**, 4262–4267;
76 L. Messori, F. Abbate, G. Marcon, P. Orioli, M. Fontani, E. Mini, T. Mazzei, S. Carotti, T. O'Connell and P. Zanello, *J. Med. Chem.,* 2000, **43**, 3541–3548;
77 M. Monim-ul-Mehboob, M. Altaf, M. Fettouhi, A. A. Isab, M. I. M. Wazeer, M. N. Shaikh and S. Altuwaijri, *Polyhedron*, 2013, **61**, 225–234;
78 F. Abbate, P. Orioli, B. Bruni, G. Marcon and L. Messori, *Inorg. Chim. Acta*, 2000, **311**, 1–5;
79 M. C. Gimeno, J. M. López-de-Luzuriaga, E. Manso, M. Monge, M. E. Olmos, M. Rodríguez-Castillo, M.-T. Tena, D. P. Day, E. J. Lawrence and G. G. Wildgoose, *Inorg. Chem.*, 2015, **54**, 10667–10677;
80 G. Marcon, S. Carotti, M. Coronnello, L. Messori, E. Mini, P. Orioli, T. Mazzei, M. A. Cinellu and G. Minghetti, *J. Med. Chem.,* 2002, **45**, 1672–1677;
81 E. M. A. Ratilla, H. M. Brothers II and N. M. Kostic, *J. Am. Chem. Soc.,* 1987, **109**, 4592–4599;
82 J. F. Michalec, S. A. Bejune, D. G. Cuttell, G. C. Summerton, J. A. Gertenbach, J. S. Field, R. J. Haines and D. R. McMillin, *Inorg. Chem.*, 2001, **40**, 2193–2200;
83 D. R. McMillin and J. J. Moore, *Coord. Chem. Rev.*, 2002, **229**, 113–121;
84 D. K. Crites, C. T. Cunningham and D. R. McMillin, *Inorg. Chim. Acta,* 1998, **273**, 346–353;
85 R. Büchner, C. T. Cunningham, J. S. Field, R. J. Haines, D. R. McMillin and G. C. Summerton, *J. Chem. Soc., Dalton Trans.,* 1999, 711–718;
86 H.-K. Yip, L.-K. Cheng, K.-K. Cheung and C.-M. Che, *J. Chem. Soc., Dalton Trans*., 1993, 2933–2938;
87 J. F. Michalec, S. A. Bejune and D. R. McMillin, *Inorg. Chem.,* 2000, **39**, 2708–2709;
88 G. Wilkinson, R. D. Gillard and J. A. McCleverty, *Comprehensive coordination chemistry: the synthesis, reactions, properties & applications of coordination compounds. Main group and early transition elements*, Pergamon Press, 1987;
89 I. Uçar, A. Bulut and O. Büyükgüngör, *J. Phys. Chem. Solids*, 2007, **68**, 2271–2277;
90 B. J. Hathaway and D. E. Billing, *Coord. Chem. Rev.,* 1970, **5**, 143–207;
91 P. M. Olsen, C. Ruiz, D. Lussier, B. K. Le, N. Angel, M. Smith, C. B. Hwang, R. Khatib, J. Jenkins, K. Adams, J. Getcher, F. Tham, Z. G. Chen, E. H. Wilson and J. F. Eichler, *J. Inorg. Biochem.,* 2014, 141, 121–131;
92 A. N. Wein, A. T. Stockhausen, K. I. Hardcastle, M. R. Saadein, S. B. Peng, D. Wang, D. M. Shin, Z. G. Chen and J. F. Eichler, *J. Inorg. Biochem.,* 2011, 105, 663–668;
93 b M. J. Frisch, G. W. Trucks, H. B. Schlegel, G. E. Scuseria, M. A. Robb, J. R. Cheeseman, G. Scalmani, V. Barone, B. Mennucci, G. A. Petersson, H. Nakatsuji, M. Caricato, X. Li, H. P. Hratchian, A. F. Izmaylov, J. Bloino, G. Zheng, J. L. Sonnenberg, M. Hada, M. Ehara, K. Toyota, R. Fukuda,J. Hasegawa, M. Ishida, T. Nakajima, Y. Honda, O. Kitao, H. Nakai, T. Vreven, J. A. Montgomery Jr., J. E. Peralta, F. Ogliaro, M. Bearpark, J. J. Heyd, E. Brothers, K. N. Kudin, V. N. Staroverov, R. Kobayashi, J. Normand, K. Raghavachari, A. Rendell, J. C. Burant, S. S. Iyengar,J. Tomasi, M. Cossi, N. Rega, J. M. Millam, M. Klene, J. E. Knox, J. B. Cross, V. Bakken, C. Adamo, J. Jaramillo, R. Gomperts, R. E. Stratmann, O. Yazyev, A. J. Austin,R. Cammi, C. Pomelli, J. W. Ochterski, R. L. Martin, K. Morokuma, V. G. Zakrzewski, G. A. Voth, P. Salvador, J. J. Dannenberg, S. Dapprich, A. D. Daniels, Ö. Farkas, J. B. Foresman, J. V. Ortiz, J. Cioslowski and D. J. Fox, Gaussian, Inc., Wallingford CT, 2009
94 E. Sakuda, A. Funahashi and N. Kitamura, *Inorg. Chem.*, 2006, **45**, 10670–10677;
95 E. A. Medlycott and G. S. Hanan, *Chem. Soc. Rev.*, 2005, **34**, 133–142;
96 L. M. Hight, M. C. McGuire, Y. Zhang, M. A. Bork, P. E. Fanwick, A. Wasserman and D. R. McMillin, *Inorg. Chem.,* 2013, **52**, 8476−8482;
97 C. Bronner and O. S. Wenger, *Dalton Trans.,* 2011, **40**, 12409–12420;
98 H.-Q. Liu, T.-C. Cheung, S.-M. Peng and C.-M. Che, *J. Chem. Soc. Chem. Commun.*, 1995, 1787–1788;
99 T. K. Aldridge, E. M. Stacey and D. R. McMillin, *Inorg. Chem*., 1994, **33**, 722–727;
100 V. K.-M. Au, K. M.-C. Wong, D. P.-K. Tsang, M.-Y. Chan, N. Zhu and V. W.-W. Yam, *J. Am. Chem. Soc.,* 2010, **132**, 14273–14278;
101 K. T. Chan, G. S. M. Tong, W.-P. To, C. Yang, L. Du, D. L. Phillips and C.-M. Che, *Chem. Sci.*, 2017, **8**, 2352–2364;
102 Y.-C. Chang, K.-C. Tang, H.-A. Pan, S.-H. Liu, I. O. Koshevoy, A. J. Karttunen, W.-Y. Hung, M.-H. Cheng and P.-T. Chou, *J. Phys. Chem. C,* 2013, **117**, 9623−9632;
103 C.-C. Hsu, C.-C. Lin, P.-T. Chou, C.-H. Lai, C.-W. Hsu, C.-H. Lin and Y. Chi, *J. Am. Chem. Soc.,* 2012, **134**, 7715−7724;
104 Y.-M. Cheng, Y.-S. Yeh, M.-L. Ho, P.-T. Chou, P.-S. Chen and Y. Chi, *Inorg. Chem.*, 2005, **44**, 4594–4603;
105 D. N. Kozhevnikov, V. N. Kozhevnikov, M. Z. Shafikov, A. M. Prokhorov, D. W. Bruce and J. A. G. Williams, *Inorg. Chem.*, 2011, **50**, 3804–3815;

Published on 04 April 2018. Downloaded by Fudan University on 04/04/2018 08:52:59.
Dalton Transactions Accepted Manuscript

This journal is © The Royal Society of Chemistry 20xx

Please do not adjust margins
View Article Online
DOI: 10.1039/C8DT00558C

106 H. Weissman, E. Shirman, T. Ben-Moshe, R. Cohen, G. Leitus, L. J. W. Shimon and B. Rybtchinski, *Inorg. Chem.,* 2007, **46**, 4790–4792;
107 W. Y. Heng, J. Hu and J. H. K. Yip, *Organometallics*, 2007, **26**, 6760–6768;
108 106. S. Lentijo, J. A. Miguel and P. Espinet, *Inorg. Chem.,* 2010, **49**, 9169–9177;
109 V. Prusakova, C. E. McCusker and F. Castellano, *Inorg. Chem.,* 2012, **51**, 8589–8598;
110 S. Lentijo, G. Aullon, J. A. Miguel and P. Espinet, *Dalton Trans.,* 2013, **42**, 6353–6356;
111 M. Serratrice, M. A. Cinellu, L. Maiore, M. Pilo, A. Zucca, C. Gabbiani, A. Guerri, I. Landini, S. Nobili, E. Mini and L. Messori, *Inorg. Chem.,* 2012, **51**, 3161−3171;
112 M. H. Wilson, L. P. Ledwaba, J. S. Field and D. R. McMillin, *Dalton Trans.,* 2005, 2754–2759;
113 J. S. Field, R. J. Haines, L. P. Ledwaba, R. McGuire, Jr., O. Q. Munro, M. R. Low and D. R. McMillin, *Dalton Trans.,* 2007, 192–199;
114 A. Maroń, K. Czerwińska, J. G. Małecki, B. Machura, A. Szlapa-Kula and S. Krompiec, *ChemistrySelect*, 2017, **2**, 1071–1078;
115 W.-W. Yam, R. P.-L. Tang, K. M.-C. Wong and K.-K. Cheung, *Organometallics,* 2001, **20***,* 4476–4482;
116 D. Ma, L. Duan and Y. Qiu, *Dalton Trans.,* 2015, **44**, 8521–8528;
117 R. D. Rakhimov, Yu. A. Weinstein, E. V. Lileeva, N. N. Zheligovskaya, M. Ya. Mel'nikov and K. P. Butin, *Russ. Chem. Bull., Int. Ed.,* 2003, **52**, 1150–1156;
118 Q.-Z. Yang, L.-Z. Wu, Z.-X. Wu, L.-P. Zhang and C.-H. Tung, *Inorg. Chem.,* 2002, **41**, 5653–5655;
119 K. M.-C. Wong, W.-S. Tang, B. W.-K. Chu, N. Zhu and V. W.-W. Yam, *Organometallics,* 2004, **23***,* 3459–3465;
120 X. Liu, E. J. L. McInnes, C. A. Kilner, M. Thornton-Pett and M. A. Halcrow, *Polyhedron*, 2001, **20**, 2889–2900;
121 T. Zou, C. T. Lum, C.-N. Lok, J.-J. Zhang and C.-M. Che, *Chem. Soc. Rev.,* 2015, **44**, 8786–8801;
122 T. F. S. Silva, P. Smoleński, L. M. D. R. S. Martins, M. F. C. Guedes da Silva, A. R. Fernandes, D. Luis, A. Silva, S. Santos, P. M. Borralho, C. M. P. Rodrigues and A. J. L. Pombeiro, *Eur. J. Inorg. Chem.,* 2013, 3651–3658;
123 L. Vela, M. Contel, L. Palomera, G. Azaceta and I. Marzo, *J Inorg Biochem.,* 2011, **105**, 1306–1313;
124 U. Jungwirth, C. R. Kowol, B. K. Keppler, C. G. Hartinger, W. Berger and P. Heffeter, *Antioxid Redox Signal.,* 2011, **15**, 1085–1127;
125 J. Wang and G. S. Hanan, *Synlett.,* 2005, **8**, 1251–1254;
126 A. N. Kharat, A. Bakhoda and S. Zamanian, *Polyhedron*, 2011, **30**, 1134–1142;
127 E. C. Constable, E. L. Dunphy, C. E. Housecroft, M. Neuburger, S. Schaffner, F. Schaper and S. R. Batten, *Dalton Trans.*, 2007, 4323–4332;
128 U. Resch-Genger, Y. Q. Li, J. L. Bricks, V. Kharlanov and W. Rettig, *J. Phys. Chem. A*, 2006, **110**, 10956–10971;
129 W. Spahni and G. Calzagerri, *Helv. Chim. Acta*, 1984, **67**, 450–454;
130 R. N. Keller and T. Moeller, *Inorg. Synth.*, 1963, **7**, 242–250;
131 Oxford Diffraction. *CrysAlis PRO.*, Oxford Diffraction Ltd, Yarnton, England, 2011;
132 G. M. Sheldrick, *Acta Cryst. C,* 2015, **71**, 3–8;
133 P. Perdew, K. Burke and M. Ernzerhof, Phys. Rev. Lett. , 1996, **77**, 3865–3868
134 M. Ernzerhof and G.E. Scuseria, J. Chem. Phys., 1999, **110**, 5029–5036;
135 C. Adamo and V. Barone, *J. Chem. Phys.*, 1999, **110**, 6158–6169;
136 D. Andrae, U. Haussermann, M. Dolg, H. Stoll and H. Preuss, *Theor. Chim. Acta*, 1990, **77**, 123–141;
137 F. Weigend and R. Ahlrichs, *Phys. Chem. Chem. Phys.*, 2005, **7**, 3297–3305;
138 F. Weigend, *Phys. Chem. Chem. Phys.*, 2006, **8**, 1057–1065;
139 M. Dolg, H. Stoll, H. Preuss and R.M. Pitzer, *J. Phys. Chem.*, 1993, **97**, 5852–5859;
140 B. Mennucci and J. Tomasi, *J. Chem. Phys.*, 1997, **106**, 5151–5158;
141 M. T. Cances, B. Mennucci and J. Tomasi, *J. Chem. Phys.*, 1997, **107**, 3032–3041;
142 M. Cossi, V. Barone, B. Mennucci and J. Tomasi, *Chem. Phys. Lett.*, 1998, **286**, 253–260.

Published on 04 April 2018. Downloaded by Fudan University on 04/04/2018 08:52:59.
Dalton Transactions Accepted Manuscript

Please do not adjust margins

View Article Online
DOI: 10.1039/C8DT00558C

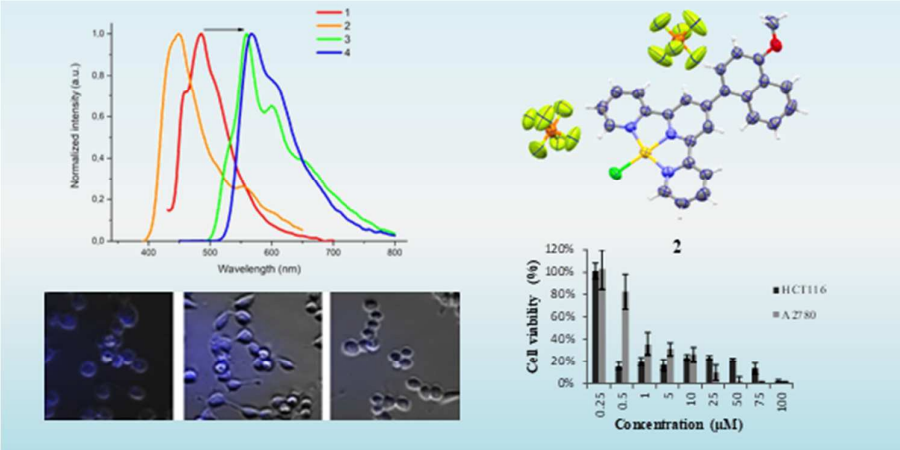

Spectroscopy, electrochemistry and antiproliferative properties of Au(III), Pt(II) and Cu(II) complexes bearing modified 2,2′:6′,2″-terpyridine ligands have been investigated and impact of metal center and substituent incorporated into terpy framework have been demonstrated.

Published on 04 April 2018. Downloaded by Fudan University on 04/04/2018 08:52:59.

Dalton Transactions Accepted Manuscript